الجمهورية الجزائرية الديمقراطية الشعبية
République Algérienne Démocratique et Populaire
وزارة التعليم العالي والبحث العلمي
Ministère de l'enseignement supérieur et de la recherche scientifique

Université Mohamed Khider – Biskra
Faculté des Sciences et de la Technologie
Département de Génie Civil et Hydraulique
Référence : ……….

جامعة محمد خيضر – بسكرة
كلية العلوم والتكنولوجيا
قسم الهندسة المدنية والري
المرجع: ....

Thèse présentée en vue de l'obtention du diplôme de

Doctorat LMD en Travaux Publics

Option : Voies et Ouvrages d'Arts

Analysis of the static and dynamic thermomechanical behavior of FGM and sandwich beams

Analyse du comportement thermomécanique statique et dynamique des poutres FGM et sandwich

Présenté par

Abdelhamid Benzid

Soutenue publiquement le : 06/04/2025

Devant le jury composé de :

Djamal Hamadi	Professeur	Président	Université de Biskra
Abdelouahab TATI	Professeur	Rapporteur	Université de Biskra
Lakhdar Sedira	Professeur	Examinateur	Université de Biskra
Mohamed Guenfoud	Professeur	Examinateur	Université de Guelma
Mohamed-Ouejdi Belarbi	Professeur	Examinateur	Université de Biskra
Abderahim Belounar	MCA	Examinateur	Centre U. de Tipaza

“*To My Dear Parents, Wife, Brothers, Sisters, and My Daughter Rym Safia*”

Acknowledgements

First and foremost, I express my deepest gratitude to Allah, without Allah divine guidance and mercy this thesis would not have been possible. His endless blessings have given me the strength, knowledge, and ability to complete this scholarly work.

I would like to express my sincere gratitude to my supervisor, Abdelouahab Tati, whose expertise, insight, and patience have been instrumental in shaping both this research and my development as a scholar. Their mentorship went beyond academic guidance, teaching me the true essence of scientific inquiry and critical thinking.

I am deeply thankful to all the jury members, Mr. Djamal Hamadi, Professor at the University of Biskra, Mr. Lakhdar SEDIRA, Professor at the University of Biskra, Mr. Mohamed Guenfoud, Professor at the University of Guelma, Mr. Mohamed-Ouejdi Belarbi, MCA at the University of Biskra, and Mr. Abderahim Belounar, MCA at university center of Tipaza for accepting to review my thesis.

I gratefully acknowledge all professors and administrative staff of Mohamed Khider University and the Department Civil Engineering and Hydraulics, who have been extraordinarily helpful throughout my research. Particular thanks go to Mrs. Selma Haouara for their administrative support.

On a personal note, I am deeply grateful to my family for their unwavering support and understanding throughout this challenging journey. To my parents, thank you for instilling in me the value of education and perseverance. To my wife, your patience, encouragement, and support have been my anchor throughout this process.

Finally, I would like to thank everyone who directly or indirectly contributed to making this thesis possible. This achievement is as much yours as it is mine.

Abdelhamid Benzid

Abstract

This work presents a new high-order shear deformation theory using the enhanced Timoshenko beam theory (ETBT) to analyze FGM beams' behaviors. The developed model exhibits a quadratic distribution of shear stress along the thickness and meets the zero-shear stress condition at both the top and bottom surfaces of the beam without using the shear correction factor. Based on the proposed model, a two-nodded finite element is formulated to analyze FG and sandwich beams' static, buckling, and free vibration behaviors. This element has only three unknowns, unlike other higher-order models, which use a great number of variables. The stiffness and geometrical matrices have been derived using the principle of total potential energy. The concept of a physical neutral axis is introduced to avoid the stretching-bending phenomenon. The accuracy and the performance of the proposed model have been confirmed through comparisons with the results of the existing literature. In addition, the effect of the power law index, length-to-thickness ratio, and boundary conditions on displacement, stresses, critical temperature and buckling load, and natural frequencies is investigated. The obtained results indicate that the formulated finite element is reliable for predicting the static, buckling, and free vibration behaviors of FGM beams.

Keywords: Functionally graded materials, beams, Static, buckling, free vibration, Timoshenko beam theory, Finite element method, Neutral axis.

ملخص

يقدم هذا العمل نظرية تشوّه قص جديدة عالية الدرجة باستخدام نظرية عوارض تيموشينكو المحسّنة لتحليل سلوك العوارض المتدرجة وظيفياً. يُظهر النموذج المطور توزيعًا تربيعيًا لإجهاد القص على طول السُمك ويفي بشرط إجهاد القص الصفري عند كل من السطحين العلوي والسفلي للعارضة دون استخدام معامل تصحيح القص. استناداً إلى النموذج المقترح، تمت صياغة عنصر محدود ثنائي العقد لتحليل السلوكيات الاستاتيكي والالتواء والاهتزاز الحر للعوارض المتدرجة وظيفياً والعوارض الساندويتش. يحتوي هذا النموذج على ثلاثة مجاهيل فقط، على عكس النماذج الأخرى ذات الدرجة الأعلى، والتي تستخدم عددًا كبيرًا من المتغيرات. تم اشتقاق مصفوفات الصلابة والمصفوفات الجيومترية باستخدام مبدأ الطاقة الكامنة الكلية. تم إدخال مفهوم المحور المحايد الفيزيائي لتجنب ظاهرة التمدد والانحناء. تم تأكيد دقة وأداء النموذج المقترح من خلال مقارنات مع نتائج الدراسات السابقة. بالإضافة إلى ذلك، تم دراسة تأثير مؤشر قانون القوة ونسبة الطول إلى السماكة والظروف الحدية على الإزاحة والإجهادات ودرجة الحرارة الحرجة وحمل التواء الحرج والترددات الطبيعية. تشير النتائج التي تم الحصول عليها إلى أن النموذج المقترح يمكن الاعتماد عليه للتنبؤ بالسلوكيات الاستاتيكية والالتواء والاهتزاز الحر لعوارض المواد المتدرجة وظيفياً.

الكلمات المفتاحية: المواد المتدرجة وظيفياً، العوارض، الانحناء، الثبات، الاهتزاز الحر، نظرية تيموشينكو للعوارض، طريقة العناصر المحدودة، المحور المحايد.

Publications and Communication List

International Publication

- **Abdelhamid Benzid** & Abdelouahab Tati (23 Oct 2023): Static and buckling behaviors analysis of FG beams using a three unknowns finite element based on enhanced Timoshenko theory, Mechanics of Advanced Materials and Structures, DOI: 10.1080/15376494.2023.2270969

International Communications

- **Abdelhamid Benzid** & Abdelouahab Tati. Finite element model for buckling behavior of functionally graded beams based on modified Timoshenko beam theory. in The Third International Civil Engineering Seminar of Bechar. 15-16/11/2023. Bechar- Algeria.
- **Abdelhamid Benzid** & Abdelouahab Tati. A Novel Finite element model For Static bending Analysis Of Functionally Graded Beams. Second Arab Conference on Mechanics & Engineering. 10-12/12/2023. Biskra- Algeria.
- **Abdelhamid Benzid** & Abdelouahab Tati. Thermal buckling analysis of Functionally graded material beams. 1st international conference on water, energy, environment and material engineering. 10-11/12/2024. Ouargla-Algeria.

National Communications

- **Abdelhamid Benzid** & Abdelouahab Tati. A High-order beam theory for bending analysis of functionally graded beams. The First National Conference on Mechanical Engineering. 10/05/2023. Batna- Algeria.
- **Abdelhamid Benzid** & Abdelouahab Tati. Numerical analysis of Static behavior of functionally graded material beams. First National Conference on Advanced Materials and Their Application. 18-19/10/2023. Tipaza- Algeria.

Table of Contents

List of Tables

List of Figures

List of Symbols and Abbreviations

Symbols

A, D, H	Elastic coefficient
b	Width of the beam
C-C	Clamped-Clamped beam
C-F	Clamped-Free beam
E	Young's modulus
e	Distance between the neutral axis and the centroid
F	Distributed load
$f(z)$, $\Gamma(z)$	The shear function
$\{F_e\}$	Nodal Load vector
h	Total thickness (depth) of the beam
h_0, h_1, h_2, h_3	Layer thickness (depth)
I_0 and I_2	Moment of inertia
$[I]$	Inertia matrix
$[K_e]$	Elementary stiffness matrix
$[K_e^g]$	Elementary geometric matrix
L	Length of the beam
L/h	Length-to-thickness (depth) ratio
$[M]$	Mass matrix
$[B_a],[B_b],[B_s]$	Axial, bending, and shear strain matrices respectively
M_x	Moment resultants
$[N]$	Shape functions matrix
N_i	Lagrange shape function
N_x	Normal stress resultants
k_x	Curvature
$P(z)$	Material property
p	Power law index / volume fraction exponent
P_0	Mechanical load

$\bar{P}_{cr}$	Dimensionless critical buckling load
$\{q\}$	Displacement vector
Q	Stiffness coefficient
S_{xz}	Transverse shear stress resultants
$S\text{-}S$	Simply supported beam
T	Kinetic energy
t	Time
U	Strain energy
u , w	Displacement vector Component
u_0 , w_0	Displacement Component of center axis
V	Beam's volume
V_c	Volume fraction
$\bar{w}$	Nondimensional displacement
W	External loads work
α	Thermal expansion coefficient
ΔT	Temperature rise
ΔT_{cr}	Critical temperature
ε_T	Strain due temperature rise
ε_x^0	Axial strain
ε^{nl}	Nonlinear strain
χ_x , θ_x	High-order functions
γ_{xz}^0	Shear strain
λ	Loading factor
ν	Poisson's ratio
ω	Natural frequency
$\bar{\omega}$	Dimensionless natural frequencies
Ω	Beam's surface
φ_x	Transverse normal rotations about the y axis
ψ_z	Stretching contribution
ρ	Density
σ_x, σ_{xz}	Normal and Shear stress respectively
$\bar{\sigma}_x$, $\bar{\sigma}_{xz}$	Nondimensional Normal and Shear stress respectively

Abbreviations

1D	One Dimension
2D	Two Dimensions
3D	Three Dimension
AM	Additive Manufacturing
ASDT	Aydogdu Shear Deformation Theory
CBT	Classic Beam Theory
CVD	Chemical Vapor Deposition
CUF	Carrera Unified Formulation
DOF	Degrees Of Freedom
DQM	Differential Quadrature Method
E-FGM	Exponential Law
EBBT	Euler-Bernoulli Beam Theory
ETBT	Enhanced Timoshenko Beam Theory
ESDT	Exponential Shear Deformation Theory
FE /M	Finite Element /Method
FDM	Fused Deposition Modeling
FG /M	Functionally Graded /Materials
FSDT	First-Order Shear Deformation Theory
FVM	Finite Volume Method
HOZT	High-Order Zigzag Theory
HSDBT	Hyperbolic Shear Deformation Beam Theory
HSDT	High-order Shear Deformation Theory
LBT	Levinson Beam Theory
LE	Lagrangian Extension
P-FGM	Power-Law
PM	Powder Metallurgy
PVD	Physical Vapor Deposition
RSDT	Refined Shear Deformation Theory
RZT	Refined Zigzag Theory
S-FGM	Sigmoid Law
SCF	Shear Correction Factor
SSDBT	Sinusoidal Shear Deformation Beam Theory
SSDT	Second-Order Shear Deformation Theory
SSPH	Symmetric Smoothed Particle Hydrodynamics
TBT	Timoshenko Beam Theory
TSDT	Third-Order Shear Deformation Theory
UDL	Uniform Distributed Load
UI	Unified and Integrated

General Introduction

In the pursuit of developing super-heat-resistant materials, Japanese materials scientists proposed the concept of Functionally Graded Materials (FGMs) in the early 1980s. These materials, microscopically heterogeneous and typically made up of isotropic components such as metals and ceramics, were initially conceived as thermal barriers for aerospace structures and fusion reactors. Compared with traditional composites, FGMs offer various advantages, such as ensuring a smooth transition in stress distribution, minimizing or eliminating stress concentration and increasing bond strength along the interface of two different materials. On the other hand, over the past two decades, FGMs have been widely applied in modern industries including aerospace, mechanical engineering, electronics, optics, chemistry, biomedical, nuclear and civil engineering, to name but a few. Motivated by these engineering applications, FGMs have also attracted intensive research interest, mainly focused on their static, dynamic and stability behaviors. Furthermore, structural elements such as beams, plates and shells are commonly used. Consequently, understanding their behavior is necessary for practical applications.

Thesis objective

This doctoral research aims to develop a new model and numerically analyze functionally graded and sandwich beams behaviors through different parameters and boundary conditions, with a particular focus on improving the accuracy and predictive capabilities of the proposed model.

Thesis organization

This thesis is presented in two main parts:

Part one: Literature review

The first chapter discusses FGMs, covering their fundamental characteristics, historical development, and type of gradation. It also explores different categories of FGMs such as Chemical Compositional, Porosity, and Microstructural Gradation, and examines processing methods and material gradation rules essential for designing and modeling FGM properties.

In chapter two, initially we presented the most employed theories in analyzing and modelling FGM beams, as well as an overview of the approaches, theories and various models use to analyze the behaviors of FG and sandwich beams.

Part two: Development of new finite element model based on enhanced Timoshenko beam theory

The third chapter is dedicated to theorical development of new enhanced Timoshenko beam theory (ETBT) for analyzing FGM beams. The proposed model uses three unknowns, incorporates quadratic shear strain distribution, and meets zero shear stress conditions. As well as, formulating a new finite element for the static, buckling, and free vibration responses considering thermal effects and material properties variation through the depth.

The fourth chapter conducts numerical analysis of the developed ETBT model, assessing its convergence, accuracy, and stability. It explores various FG beams response including static, buckling, and free vibration behaviors. The model is validated by comparing results with existing research and examining the influence of different parameters on FG beams behaviors

The fifth chapter presents numerical examples evaluating the developed finite element's performance in analyzing FG sandwich beams. Focuses on buckling and free vibration behaviors. The results are validated against existing literature, with an exploration of how parameters like support conditions and length-to-depth ratio influence beam characteristics.

This research end with a general conclusion, encompassing the research problem, primary objectives, and key findings, complemented by potential future research directions.

Part I Literature Review

Chapter 1:
Functionally Graded Materials

1.1. Introduction

Functionally Graded Materials or FGMs, are innovative kinds of engineered materials that maintain their properties and structural integrity in extreme conditions. Unlike other composites, in FGMs the composition changes gradually from one to another.

The concept of Functionally Graded Materials and their fundamental characteristics has been presented in this chapter. This is followed by a brief background, tracing the development of FGMs from their conceptual origins to their current state-of-the-art applications. Various types of FGMs are based on gradation, including Chemical Compositional Gradation, Porosity Gradation, and Microstructural Gradation. Each type is discussed in detail. A variety of processing methods for FGMs is also presented along with material gradation rules, which are important for modeling and designing the effective properties in FGMs.

1.2. Functionally graded material: Definition

Functionally Graded Materials are a new class of advanced composites known by gradual variations in composition, structure, and/or specific properties over one or more dimensions of the material [1, 2]. This unique attribute distinguishes FGMs from traditional composite materials, which typically exhibit abrupt transitions between distinct layers or components.

FGMs are inspired by nature, where many biological structures, such as teeth, bones, and bamboo, demonstrate gradual changes in density and composition to optimize their performance under varying conditions [3]. Inspired by these natural designs, materials scientists have created FGMs to address complex challenges in fields such as aerospace, biomedical, electronic, and other fields [4].

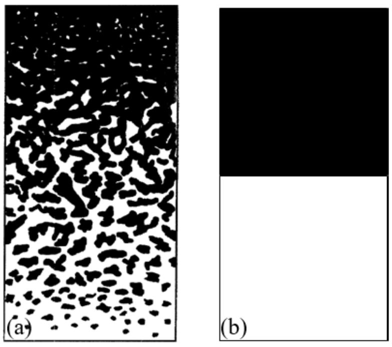

Figure 1.1 Schematic illustration of (a) FGM and (b) traditional composite material [5]

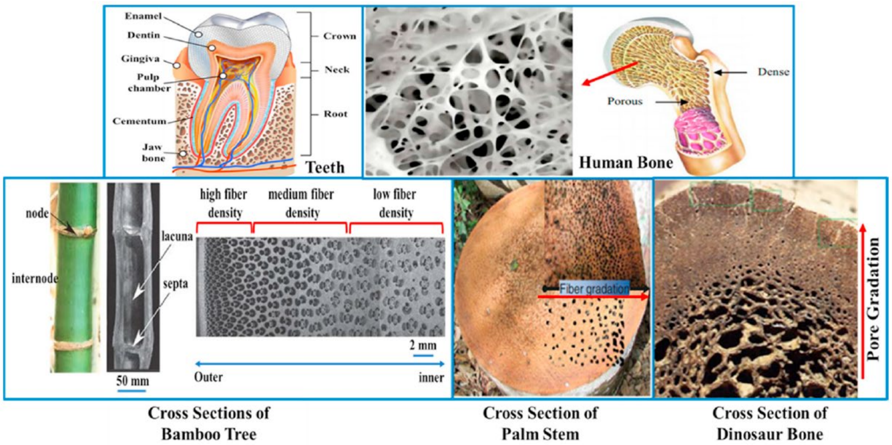

Figure 1.2 Examples of FGM in nature [6]

The principle of functionally graded materials is the variation of material properties, which can be tailored to meet specific performance requirements. This gradation can occur in terms of chemical composition, microstructure, porosity, or a combination of these factors [7, 8]. The result is a material that can exhibit a seamless transition from one set of properties to another, allowing for optimized performance across different regions of the same component [9].

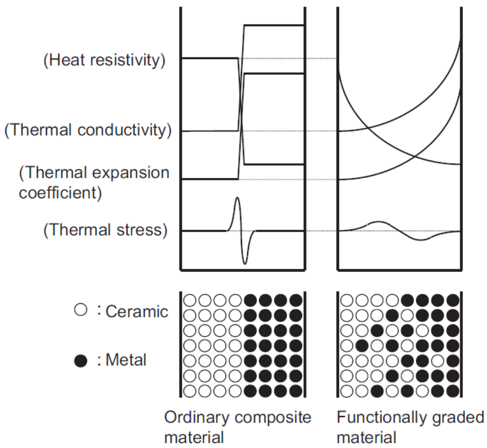

Figure 1.3 Material properties and structures of tradition composite and FGMs [10]

1.3. The Evolution of Functionally Graded Materials

The origins of FGMs go back to the 1980s, when material scientists started looking at ways of overcoming conventional composites limits. The initial inspiration came from Japan in 1984, when a spaceplane project required materials capable of resisting extreme temperature gradients of 1000 K to 2000 K at a thickness of less than 10mm [11].

Back in 1987, The term "Functionally Gradient Materials" was introduced as part of a national project on thermal barrier materials in Japan [2, 12]. This was the official birth of FGMs as a distinct field of study. During that time, the focus was on developing theoretical models and exploring potential applications, particularly in the aerospace and nuclear industries [11].

The 1990s saw substantial growth in FGM research on the global scale. During this decade, there was an increase in theoretical developments, experimental studies, and practical applications of FGMs. Researchers around the world have achieved significant progress in understanding the behavior of these materials under different conditions, focusing in particular on thermal stresses and mechanical properties [5, 13]. Further understanding of FGM behavior has led to more sophisticated designs and processing methods [14].

In the early 21st century, significant improvement has been made in FGMs fabrication technologies. Scientists have developed new methods and enhanced existing ones to produce FGMs with more complex structures and property distributions [3, 15]. Vapor deposition, centrifugal casting, and Powder metallurgy methods were refined for FGM production. These advances allowed for the creation of FGM structures with better performance and characteristics [16].

Today, FGM research continues to develop, focusing on nano-scale gradation and the integration of smart materials. Additive manufacturing has opened up new ways of creating complicated FGM structures [17, 18].

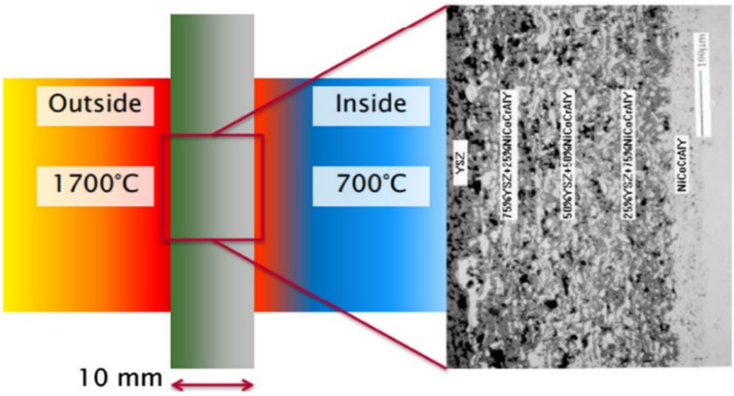

Figure 1.4 Metallic example of FGM [19]

1.4. Types of Functionally Graded Materials

The original concept behind Functionally Graded Materials emerged as a response to the limitations of conventional composite materials. The primary goal was to eliminate the abrupt transitions between different material components, replacing them with gradual, continuous changes in composition or structure. As research in this field has progressed, a diverse array of FGM types has been developed. The specific requirements of each application typically dictate the selection and design of appropriate FGM variant.

1.4.1. Chemical Compositional Gradation

Compositional gradation involves a systematic change in chemical composition across the material's volume or surface. This type of gradation allows for the seamless integration of materials with vastly different properties, such as ceramics and metals [8]. The application of chemical compositional gradation in thermal barrier coating in turbines [18].

Key features of compositional gradation include:

- Gradual transition from one material to another.
- Continuous or stepwise variation in constituent ratios.
- Ability to combine materials with contrasting properties.

1.4.2. Porosity Gradation

Porosity gradation involves controlled variation in pore size, shape, or distribution throughout the material. This approach allows engineers to tailor density, permeability, and mechanical properties while maintaining a constant chemical composition [20].

Characteristics of porosity gradation include:

- Systematic change in porosity percentage or pore size across the material.
- Control over structural properties without altering composition.
- Influence on density, permeability, and mechanical properties.

Porosity gradation has found particular success in biomedical applications, especially in the design of bone implants. Miao and Sun [20] review revealed that porosity gradients can significantly enhance cell attachment and proliferation in bone implants, with optimal pore sizes ranging from 100-400 μm .

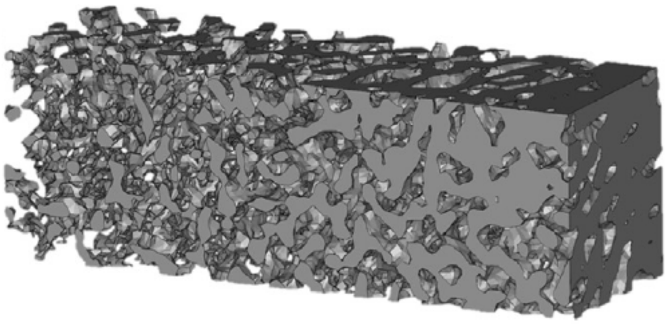

Figure 1.5 3D model of gradient structure of trabecular bone [21]

1.4.3. Microstructural Gradation

Microstructural gradation focuses on changes in the material's internal structure, such as grain size, phase distribution, or crystal structure. This approach offers a powerful means to influence mechanical, thermal, and electrical properties without necessarily altering the material's chemical composition [22].

Key aspects of microstructural gradation include:

- Gradual variation in microstructural features across the material.
- Applicability to single-phase or multi-phase materials.
- Influence on thermal, mechanical, and electrical properties.

The concept of microstructural gradients in materials was pioneered by Bever and Duwez [23], whose work on graded martensitic structures in steel laid the foundation for modern microstructural gradient design in high-performance alloys.

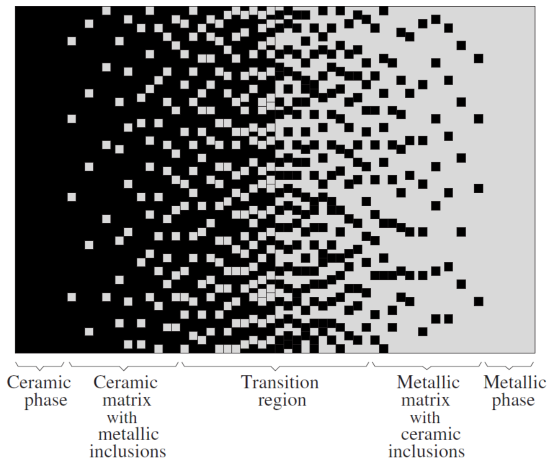

Figure 1.6 A schematic of graded microstructure [24]

1.5. Processing technique of functionally graded materials

Functionally graded materials manufacturing methods play a pivotal role, commanding significant attention from researchers. FGMs can be produced as either surface coatings or bulk materials. When applied as thin layers on material surfaces, FGMs aim to enhance the substrate's surface characteristics. Alternatively, in their bulk form, FGMs display property variations throughout their entire volume. To address the diverse needs of FGM production, researchers have developed various fabrication techniques. These methods are tailored to create either gradient surface coatings or bulk materials with continuously varying properties.

1.5.1. Vapor Deposition methods

Vapor deposition encompasses several distinct methodologies, notably Physical Vapor Deposition (PVD), Chemical Vapor Deposition (CVD), and sputter deposition. These approaches are employed in the application of gradient surface layers, yielding superior microstructural characteristics. However, their application is confined to thin-film coatings. Moreover, these techniques are characterized by high energy consumption and generate toxic gaseous byproducts [25-27]. Figure 1.7 present Schematic diagram of PVD technique and Figure 1.8 depict the experimental configuration utilized for preparing FGM by CVD.

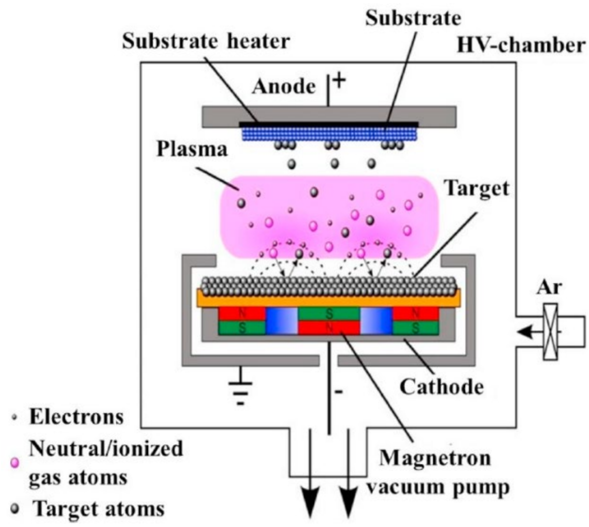

Figure 1.7 Schematic diagram of PVD technique [6]

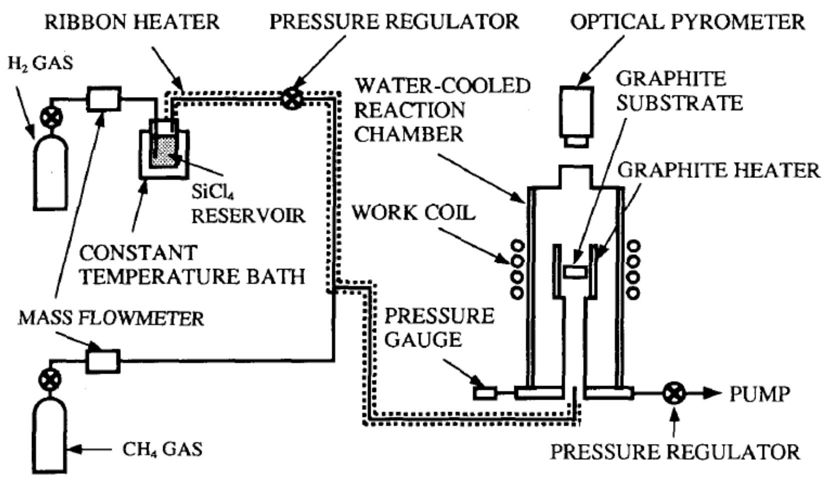

Figure 1.8 Schematic diagram of CVD Setup [26]

1.5.2. Centrifugal Method

The centrifugal method for producing functionally graded materials (FGMs) shares similarities with centrifugal casting techniques. This approach leverages gravitational forces, enhanced by the rotation of a mold, to create bulk FGMs [28, 29]. The key mechanism behind this method is the exploitation of density differences between constituent materials. As the mold spins, materials with varying densities naturally separate and distribute themselves along a gradient. This phenomenon is the cornerstone of the centrifugal method's ability to generate functionally graded structures. The resulting material exhibits a gradual change in properties and composition across its volume, directly influenced by the centrifugal forces acting on the constituent materials during the fabrication process [8, 30]. While this technique is limited to producing cylindrical shapes.

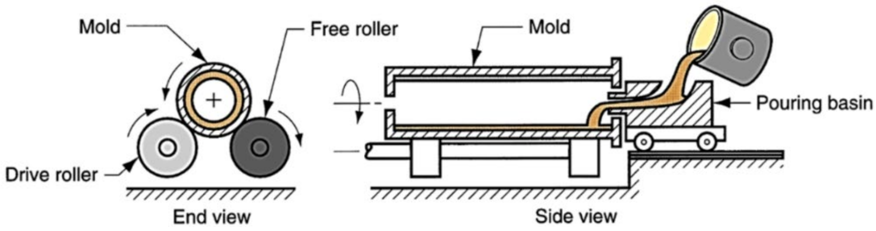

Figure 1.9 Centrifugal casting machine [31]

1.5.3. Powder metallurgy method

Powder metallurgy (PM) represents one of the oldest manufacturing processing for component production, and has recently found new application in the fabrication of FGMs [32]. Its extensive capabilities have propelled PM to the forefront of FGM production methods. As a solid-state process, PM stands out in creating bulk FGMs with discontinuous gradient properties [33, 34]. This approach is particularly valuable when discrete changes in material composition or structure are desired across the component's volume.

The PM method for FGM production typically involves four essential phases [35, 36]:

- Mixing: Combining various powder materials to achieve specific compositional ratios.
- Stacking: Layering the mixed powders to create the desired gradient structure.
- Pressing: Applying pressure to compact the layered powders into a coherent form.
- Sintering: Heat-treating the compacted material to bond particles and enhance properties.

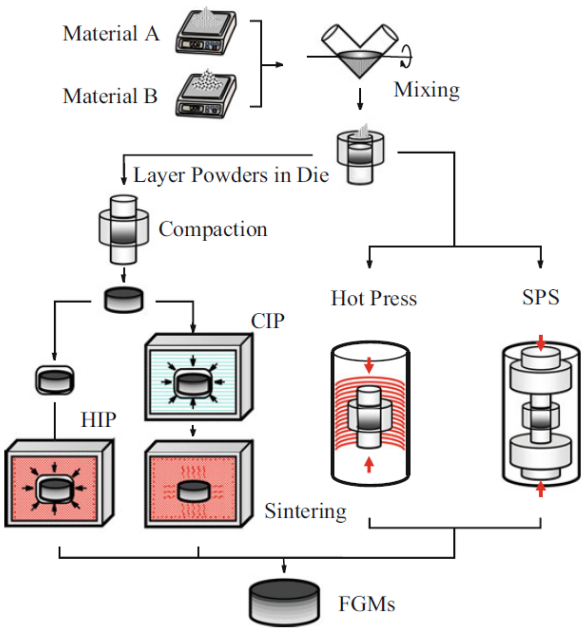

Figure 1.10 FGMs Fabrication process by PM [36]

1.5.4. Additive manufacturing methods

Additive manufacturing (AM) techniques have recently gained prominence in the fabrication of FGMs, Revolutionizing traditional metal production approaches. These methods employ sophisticated layer-by-layer machinery, significant departure from conventional molding processes [37], as illustrated in Figure 11.

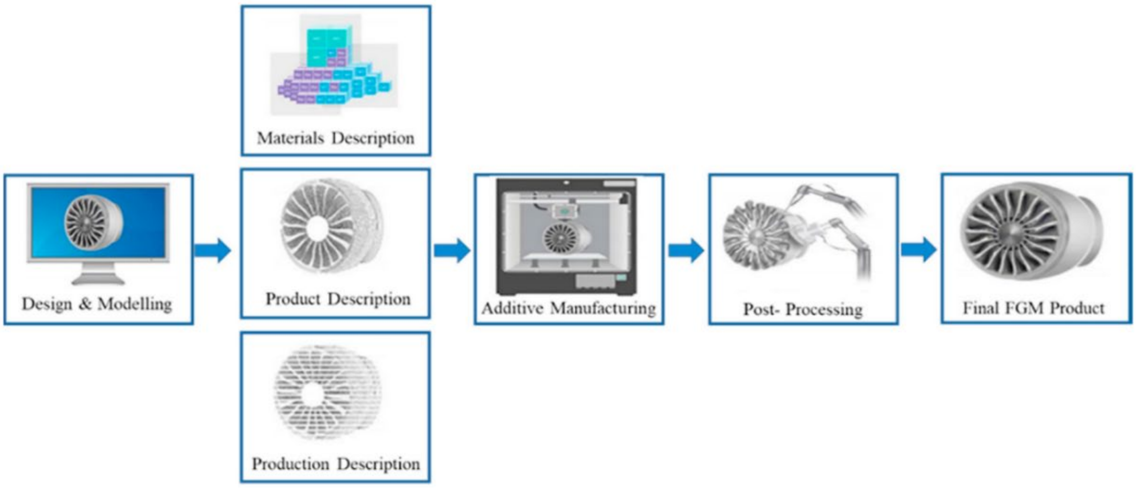

Figure 1.11 AM methods concept [37]

AM methods have recently gained traction in diverse applications, including aerospace, robotics, medical application, Architectural design, and Automotive industry. These fields increasingly demand materials with gradient properties, which AM can effectively produce by processing a range of diverse materials [38].

Several AM methods have emerged as particularly suitable for fabricating FGMs with discrete gradient. These include:

- **Material jetting:** Depositing droplets of material with high accuracy [39].
- **Laser-based methods:** Utilizing lasers for precise material deposition [40].
- **Stereolithography:** Employing light to solidify curable resins layer by layer [41].
- **Fused deposition modeling (FDM):** Often called fusion deposition simulation, this method extrudes and fuses thermoplastic material [42].

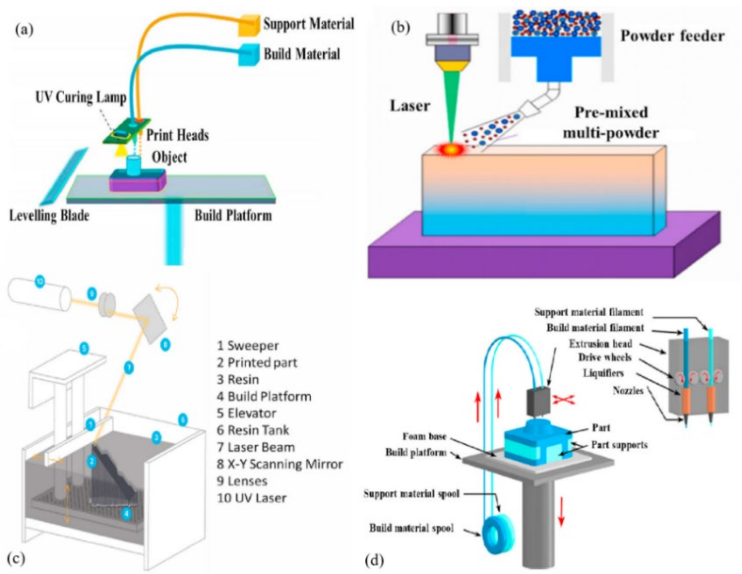

Figure 1.12 Schematic of a) Material jetting method [43]. b) Laser-based method [44]. c) Stereolithography [45]. d) Fused deposition modeling [46]

1.6. Rules for material gradation

Functionally graded materials (FGMs) are characterized by a gradual transition in structure from one material to another, resulting in a continuous variation of properties throughout the material [47, 48]. The property variations in FGMs are typically modeled using several mathematical approaches, which are Sigmoid law, Exponential law, and Power law. Figure 1.13 illustrates the geometry and coordinate systems commonly used in the analysis of FG and sandwich beams.

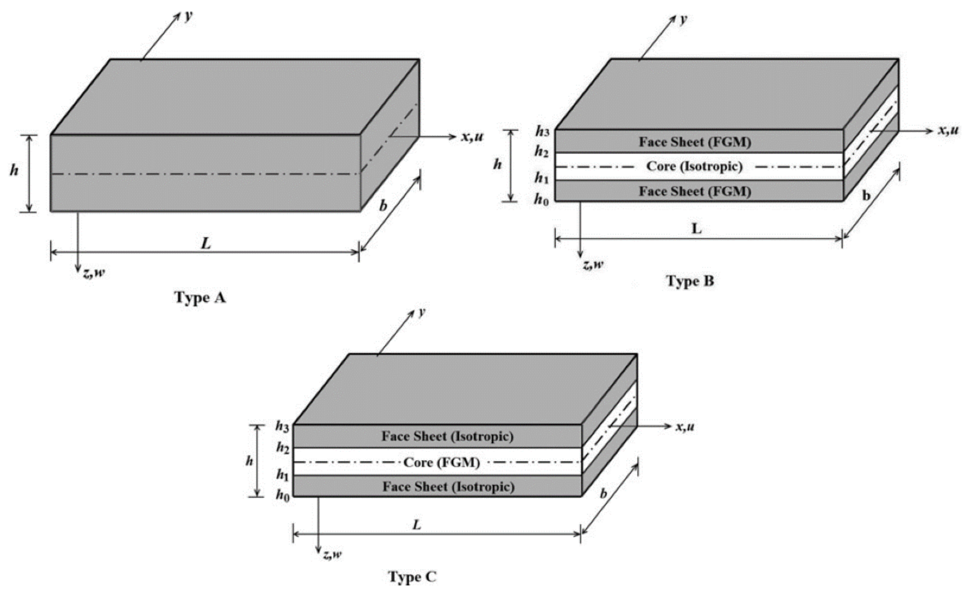

Figure 1.13 Schematic of FGM beams A) single layer FG beam. B) FG sandwich beam with homogenous core. C) FG sandwich beam with FGM core [48]

1.6.1. Power law

The power-law (P-FGM) formulation has gained significant traction among researchers in the field of functionally graded materials. It is extensively employed for modeling and analyzing FG and sandwich beams.

For FGM beams with properties varying along the thickness, the power-law can be expressed as [49] :

$$P(z) = P_2 + (P_1 - P_2)V_c \tag{1.1}$$

Where ***P*** is the material property.

The distribution of constituent materials in P-FGM can be quantified using the following volume fraction V_c expression [15]:

- Case of FG beams (type A):

$$V_c(z) = \left(\frac{1}{2} + \frac{z}{h}\right)^p \qquad z \in \left[-\frac{h}{2}, \frac{h}{2}\right] \tag{1.2}$$

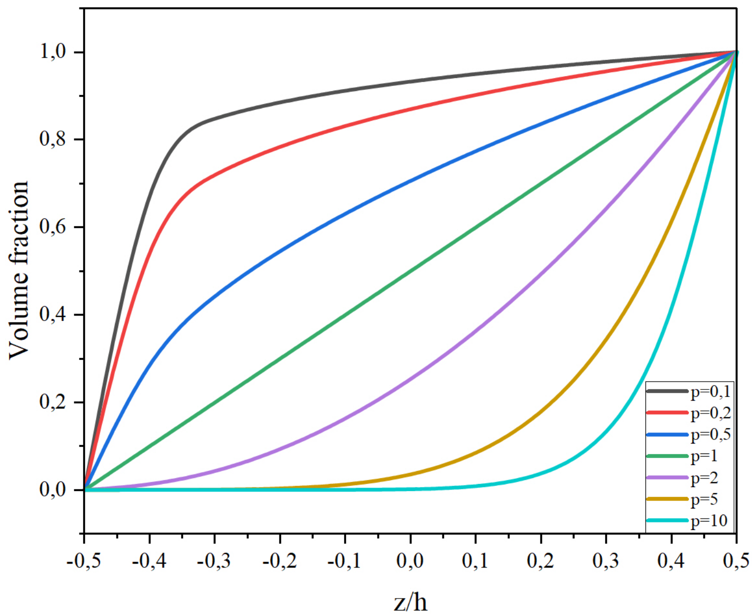

Figure 1.14 Distribution of volume fraction across the thickness of P-FGM beam

1.6.2. Exponential law

The exponential law (E-FGM) has found widespread application in fracture mechanic research. Numerous studies have employed this law to analyze both the static and dynamic characteristics of structures composed of FGM [50]. The E-FGM law is given by:

$$P(z) = P_2 e^{\frac{1}{h}\left(\ln\frac{P_1}{P_2}\right)\left(z+\frac{h}{2}\right)} \tag{1.3}$$

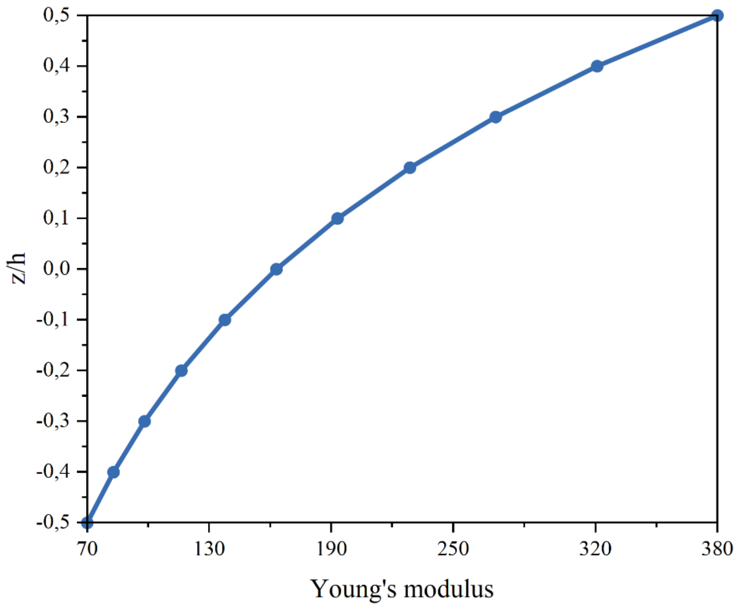

Figure 1.15 Distribution of Young's modulus across the thickness of E-FGM beam

1.6.3. Sigmoid law

The sigmoid law is a specialized material distribution model for bilayered functionally graded materials (S-FGMs). It combines two power-law functions to create a smooth property transition between layers [51]. Developed by Chung and Chi[52], this law addresses the stress discontinuity issue at layer interfaces that occurs with simple power-law models. By using two distinct power-law functions, the sigmoid law ensures stress continuity across the entire beam structure, improving the accuracy of stress predictions in bilayered FGM components. The two functions of S-FGM are expressed as follows:

$$\begin{aligned} V_{c1} &= 1-\frac{1}{2}\left(1-\frac{2z}{h}\right)^p \qquad z\in\left[0,\frac{h}{2}\right] \\ V_{c2} &= \frac{1}{2}\left(1+\frac{2z}{h}\right)^p \qquad z\in\left[-\frac{h}{2},0\right] \end{aligned} \tag{1.4}$$

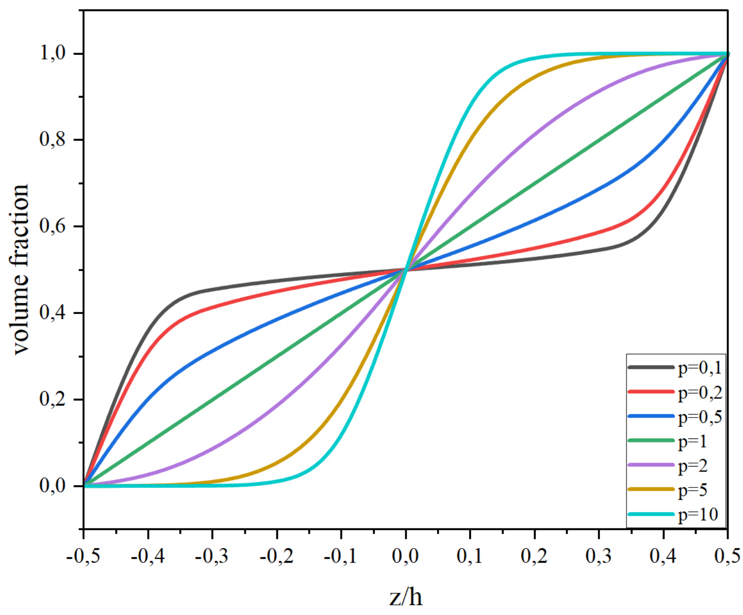

Figure 1.16 Distribution of volume fraction across the thickness of S-FGM beam

1.7. Conclusion

This chapter has presented a definition and the evolution of functionally graded materials. The various types of FGMs and their areas of application have been introduced. The main types of FGMs are chemical composition gradation, microstructure gradation, and porosity gradation. The different methods used to manufacture FGMs are discussed. These include Vapor Deposition methods for thin coating FGM; powder metallurgy, centrifugal methods, and additive manufacturing methods for bulk FGM. The gradation laws such as power law, exponential law, and sigmoid law, essential for characterizing the effective properties of functionally graded materials, are presented in this chapter.

Chapter 2:
Theories for analyzing FGM beams

2.1. Introduction

Functionally Graded Materials are advanced engineering composites combining different materials like ceramics and metals to create innovative structural elements. These materials offer superior performance in beams, plates, and shells, providing exceptional thermal stress reduction and high-temperature resistance. FGMs are typically modeled using multiple beams such as Euler-Bernoulli, Timoshenko, and higher order shear deformation theories enabling precise analysis of their behaviors. This chapter provides a comprehensive review of existing beams theories and researches focused on static, vibration, and buckling analyses of functionally graded beams.

2.2. Euler-Bernoulli beam theory

Euler-Bernoulli beam theory (EBBT) or classic beam theory (CBT), is the most used theory by engineers. This was theory developed between 1750 and 1753 by Leonhard Euler and Daniel Bernoulli [1] for thin beams. EBBT neglects the shear strain and posits that the cross-section of the beam rests orthogonal to its central axis after deformation. Moreover, it assumes that the cross-section remains planned in deformed state [53], see Figure 2.1. the displacement field of EBBT is defined as:

$$\begin{aligned} u(x,z) &= u_0(x,z) - z\frac{dw_0}{dx} \\ w(x,z) &= w_0(x,z) \end{aligned} \tag{2.1}$$

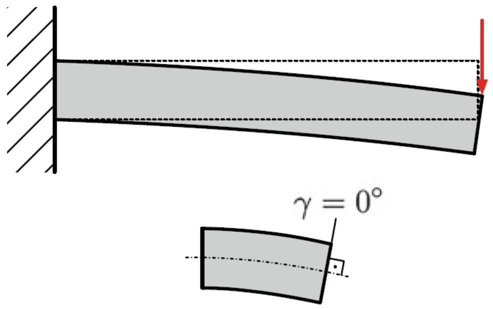

Figure 2.1 Beam's deformation according to EBBT [54]

2.3. First-order beam theory

First-order shear deformation theory (FSDT) also called Timoshenko beam theory (TBT). it overcomes the limitation of the classic beam theory by considering the effect of transverse shear stress [55]. FSDT was first introduced by Stephen Timoshenko in 1921 [56]. This approach rests on the principle that although the beam's median line preserves its straightness prior to deformation, it may not retain perpendicularity to the cross-sectional surface post-deformation (due to the effect of transverse shear) (Figure 2.2). he also assumed that the normal stress σ_y is negligible compared with the other components of the stress tensor [57-59]. The displacement field of the TBT can be written as:

$$\begin{aligned} u(x,z) &= u_0(x,z) + z\varphi_x(x,z) \\ w(x,z) &= w_0(x,z) \end{aligned} \tag{2.2}$$

From equation (2.2), we can see that the displacement components (*u*) vary linearly along the *y* axis, while the transverse displacement component (*v*) is constant. This will lead to a constant shear stress/strain through the depth of the beam , whereas, according to the theory of three-dimensional (3D) elasticity, the shear strain are rather quadratic across the thickness [60]. This limitation is corrected by the introduction of so-called shear correction factors (SCF).

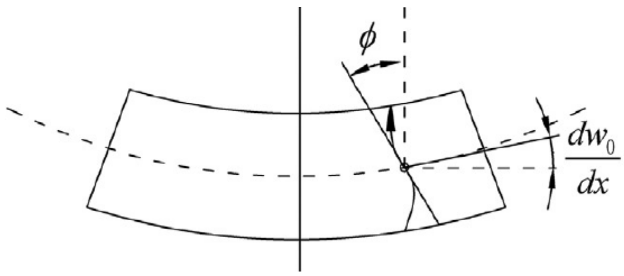

Figure 2.2 Kinematic of Timoshenko beam theory [61]

2.4. High-order beam theories

The limitation of EBBT and FSDT led researchers to develop refined approaches named High-order shear deformation theory (HSDT), these theories provides nonlinear distribution of shear stress along the beam thickness, making shear correction factor unnecessary [62-65]. Figure 2.3 shows the deformation of beam according to EBBT, FSDT, and third-order shear deformation theory (TSDT) [66].

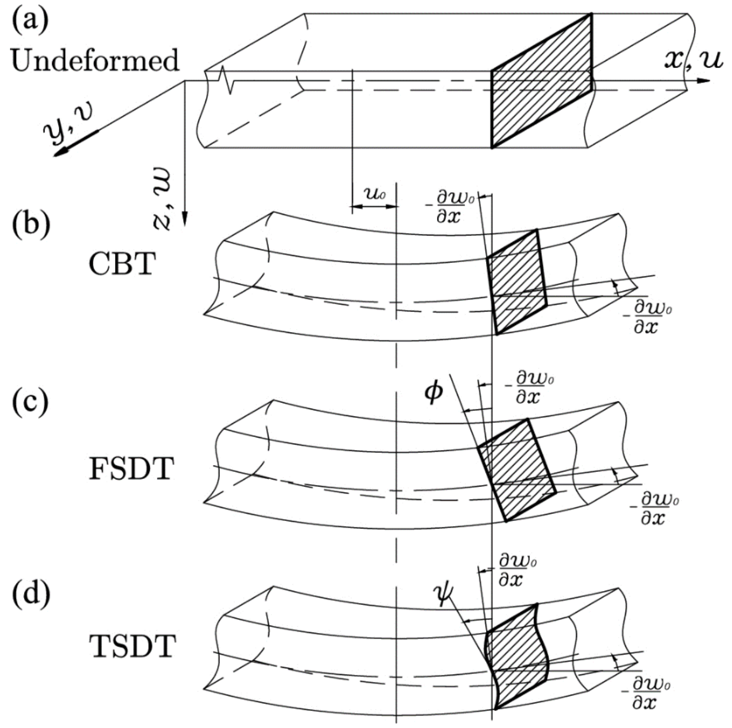

Figure 2.3 Comparison of beam deformation according to CBT, FSDT, and TSDT [66]

Many researchers have developed HSDT utilizing a power series-based approach (Taylor series expansion) to represent the displacement field. Equation provides the general expression for the displacement field [67, 68].

$$u_i\left(x, y, z, t\right) = u_i + y^j \varphi_i^j + y^{j+1} \varphi_i^{j+1} + ... + y^{j+n} \varphi_i^{j+n} \tag{2.3}$$

Where $i = \{x, y, z\}$ and j denotes the order or the power level of the theory.

For example, the Classique beam and Timoshenko beam theories corresponds to the power series up to the order j=1.

Stephen and Levinson [69] have tried to enhance the kinematics of Timoshenko by proposing the second-order shear deformation theory (SSDT) utilizing the same governing equation of FSDT but it contains two coefficients. The displacement field of SSDT is usually written as:

$$\begin{aligned} u\left(x, z\right) &= u_0(x, z) + z\varphi_x(x, z) + z^2 \kappa_x(x, z) \\ w\left(x, z\right) &= w_0(x, z) \end{aligned} \tag{2.4}$$

κ_x represent second order function.

The third-order shear deformation theory (TSDT) is an extension of EBBT and FSDT. The displacement field of TSDT contains terms up to the third-order of z [70, 71], which can be described as:

$$\begin{aligned} u(x,z) &= u_0(x,z) + z\varphi_x(x,z) + z^2\kappa_x(x,z) + y^3\theta_x(x,z) \\ w(x,z) &= w_0(x,z) \end{aligned} \tag{2.5}$$

κ_x and θ_x are high-order functions.

As the order increases, the number of variables increase. Which often become hard to interpret. To reduce the number the number of unknowns, researchers used the condition of zero shear strain at the upper and the lower face of the beam [59, 72]. Based on this simplification the displacement field can be rewritten as follows:

$$\begin{aligned} u(x,z) &= u_0(x,z) - z\frac{\partial w_0}{\partial x} + f(z)\left(\frac{\partial w_0}{\partial x} + \varphi_x\right) \\ w(x,z) &= v_0(x,z) \end{aligned} \tag{2.6}$$

The distribution of shear strain along the beam's depth is determined by the shear function $f(z)$. Furthermore, Levinson's TSDT displacement field can be derived using the following function:

$$f(z) = -\frac{4z^3}{3h^2} \tag{2.7}$$

Reddy [64] introduced an alternative TSDT by considering:

$$f(z) = z\left(1 - \frac{4z^2}{3h^2}\right) \tag{2.8}$$

Touratier [73] Developed The sinusoidal shear deformation theory (SSDT), which is obtained by taking:

$$f(z) = \frac{h}{\pi}\sin\left(\frac{z\pi}{h}\right) \tag{2.9}$$

Soldatos [74] proposed hyperbolic shear deformation beam theory (HSDBT) by setting:

$$f(y) = -z\cosh\left(\frac{1}{2}\right) + h\sinh\left(\frac{z}{h}\right) \tag{2.10}$$

Karama et al. [65] formulated exponential shear deformation theory (ESDT) by utilizing:

$$f(z) = ze^{-2\left(\frac{z}{h}\right)^2} \tag{2.11}$$

Aydogdu [75] proposed a new shear deformation theory (ASDT), which is derived by considering:

$$f(z) = z\beta^{\frac{-2\left(z/h\right)^2}{\ln\beta}} \tag{2.12}$$

These theories have been widely used by academics for accurate predicting of FGM beams behaviors. The following section reviews literatures focused on the static, buckling and vibration behaviors of FGM beams.

2.5. Previous research on modeling and analyzing FGM beams

The theoretical models for FG and sandwich beams originate from classic beam theory of Euler-Bernoulli, FSDT of Timoshenko, and various HSDTs developed over the time to improve predict the global response of these structures.

2.5.1. Static analysis

Static analysis of beams is fundamental withing structural engineering, where engineers investigate the beams response under different loads, emphasizing bending, deflection, and internal stress.

While analytic solutions are important for academics to use as a benchmark when evaluating approximate beam theory solutions, finding an exact solution for static behavior of FGM beams has proven challenging due to the difficult calculation of the problem. Sankar [76] presented a mathematical model analyzes FG beams with exponential distribution of material properties along the depth based on EBBT. According to the obtained results, the proposed model is effective for thin beams, while thick beams exhibit stress concentration. Huang et al. [77] explored the bending response of FG anisotropic cantilever beam utilizing elasticity equations for stress analysis. The authors employed a polynomial-based stress function to derive stress components through differentiation, with functions determined via compatibility equations. Zhong and Yu [78] proposed an exact solution to evaluate cantilever FGM beams under different loading conditions using stress function for a 2D solution. Where Young's modulus varies uniformly through the depth. This study provides explicit solution for specific examples to validate the proposed model. Li [79] developed a unified approach to analyze dynamic and static behaviors of FG beams, by combining rotary inertia and shear strain effects through a fourth-order differential equation that encompasses EBBT. Benatta et al. [80] used analytical solution to investigate the static behavior of simply supported FG beam under uniform loads. The obtained results are presented on beam's deflection and stresses. Ying et al. [81] introduced an analytical solution for analyzing the static and vibration response of FG Beams using 2D elasticity theory, where the material properties vary exponentially along the depth. A mathematical model transforms partial differential equations into ordinary ones using trigonometric series. The results validated were against existing literature. Giunta et al. [82] introduced refined theories for analyzing functionally graded beams, using a unified N-order formulation for displacement and deriving equations through nucleo approach. A Naiver solution is used to examine different examples under bending and torsional loads. The model's results are validated against elasticity solution and 3D finite element analysis. Ma and Lee [83] presented an exact solution for nonlinear bending response of FG beams subjected to thermal loading. Based on nonlinear FSDT, a single fourth-order integral-differential equation was derived. The exact solution were obtained for various boundary conditions. Li et al. [84] established the relationship between bending solution of FG beams based on Levinson theory and their homogenous counterparts using CBT. Analytical expression were derived for shear forces, bending moment, and deflection. The validity of this approach has been proven through comparison with previous research. Hadji et al. [85] developed a novel HSDT for analyzing the bending response of FG beams without requiring correction factor, Navier solution is used. The efficiency of the model is validated through a comparison with the existing research. Chikh [86] presented several HSDTs for analyzing static behavior of functionally graded beams. These theories satisfies zero stress condition on the upper and lower surfaces without requiring correction factor. Analytical solutions and numerical validation are presented for simply supported FG beam.

Apetre et al. [87] compared various sandwich beam theories for their applicability to 1D FG sandwich beams. Two equivalent single-layer theories, a high-order theory, and Fourier-Galerkin method are evaluated and compared to FE analysis. The results show a excellent agreement between Fourier-Galerkin method, High-order theory, and the finite element solution. Venkataraman and Sankar [88] examined the displacement and stress in a FG core of 1D sandwich beam and compare them to uniform core. Zenkour et al. [89] evaluated the static response of FG sandwich beams resting on elastic foundations. The beam faces are made of FGM and homogenous core. The obtained results are compared across different beam theories and the impacts of different parameters on stresses and deflection are also examined. Fereidoon et al. [90] analyzed the bending behavior of curved sandwich beams with FG core. In this study EBBT models the thin face, while HSDT is used for the core. The governing equations are solved using Fourier-Galerkin method. Kim and Lee [91] studied derives analytical solutions for coupled bending response of FG sandwich beams with asymmetric section. CBT and Vlasov theory were utilized for bending, and explicit expression for displacement parameters are obtained from equilibrium equation. Şimşek and Al-shujairi [92] investigated the static and dynamic behaviors of functionally graded sandwich beams employing Timoshenko theory. Three different sandwich beam models with various cross section and boundary conditions are considered. The equation of motion was solved using Newmark implicit time integration method.

The analysis of FGM structures has been conducted employing diverse analytical methods. However, these methods yield highly accurate results. These approaches are restricted to basic problems with simple geometric and boundary conditions. As result, researchers have utilized different numerical methods such as FEM to analyze FG and sandwich structures. Kadoli et al. [93] applied HSDT to evaluate the bending behavior of FG beam, employing FEM with two distinct stiffness matrices for shear and normal rotations effects. Kapuria et al. [94] validate a third-order zigzag theory for functionally graded beams utilizing the modified rule of mixtures (MROM). This research compares theoretical predictions with excremental data bending response through various boundary conditions. The results confirm both accuracy of stress-strain transfer ratio used in MROM and the Zigzag model’s effectiveness in modelling FG beams mechanics. Kocatürk et al. [95] studied the nonlinear static behavior of cantilever FGM beams using FSDT subjected to uniform loading, considering large displacement and rotation, the analysis employs a Lagrangian element with increment displacement-based FEM. The authors examine how geometric non-linearity and material distribution affect displacement and stresses. Mohanty et al. [96] analyzed bending and dynamic behavior of FG and sandwich beams employing FEM based on FSDT. This work examines how different parameters effect on the bending and dynamic stability. Vo et al. [97] carried out the static and vibration analysis of FGM beams utilizing refined shear deformation theory (RSDT) that eliminate the need for SCF. The authors developed a two-nodded element Five degrees of freedom (DOFs) per node to solve the governing equations. Filippi et al. [98] applied the 1D Carrera Unified Formulation (CUF) to analyze static behavior of FG structures, using its hierarchical feature to generate numerous displacement theories. the virtual displacements principle is used to obtain the governing equations. The problem was solved via FEM. The research evaluate different expansions across various structural conditions. A new model combining finite volume method (FVM) with Timoshenko theory was introduced by Jing et al. [99] to investigate bending and vibration response of FG beams. A three different SCF were derived utilizing Hamilton principle. The method is validated by comparing natural frequencies and deflection through diverse boundary condition and parameters, while also identifying optimal SCF. Frikha et al. [100] developed two-node element 4 DOFs per node based HSDT for studying FGM beams. The formulation uses a discrete constraint for stress-free conditions and avoids C1 displacement, presenting both displacement and mixed formulation approaches. The mixed formulation achieves accurate results even with coarse meshes, showing an excellent agreement with literatures. El-Ashmawy et al. [101] presented nonconventional FEM based on Timoshenko theory for analyzing both axially and transversally. The new model uses local constant property values per element, overcoming length dependency issues. This study includes thermal analysis in high-temperature environment. The model's accuracy comparable to HSDTs.

To investigate the static behavior FG sandwich beams numerically Vo et al. [102] developed an advanced quasi-3D that considers both thickness and shear effects, to analyze various symmetric and asymmetric beam configurations, examining how different material distribution and geometric parameters influence their mechanical response. Yarasca et al. [103] explores the bending response of FG and sandwich beams through a new 7 DOFs Quasi 3D model. The governing equations were developed utilizing virtual work principle. The kinematics variables were derived by combining cubic Hermite and linear interpolations. Karamanlı [104] examinate the static behavior of bidirectional FG sandwich beams utilizing quasi-3D and symmetric smoothed particle hydrodynamics (SSPH). Kim and Lee [105] studied flexural-torsional of thin-walled I-FG beam. the analysis consider shear and warping shear deformation, and derives governing equations utilizing total potential energy principle. The numerical results investigate the effects of boundary conditions, material ratio, gradient index, and the shear deformation on the flexural torsional of the beam. Li et al. [106] proposed novel HSDT that incorporates stress equilibrium condition, enabling the creation of new mixed FE with independent force and displacement field for precise analysis of FG sandwich beams. The mixed element demonstrated the ability to accurately evaluate displacement and stresses. Koutoati et al. [107] used 2D FG sandwich beams employing FEM, to compare the performance of CBT, FSDT, and HSDTs in predicting static and vibration response under diverse boundary conditions.

2.5.2. Buckling analysis

Buckling behavior is one of the crucial design aspects for beams subjected to compressive forces. There have been wide-ranging interest on buckling analysis of FG and sandwich beams, focusing on determining the critical bucking load and under different boundary and loading conditions.

Aydogdu [108] analyzed buckling and free vibration of axially functionally graded beam employing the semi-inverse method based on EBBT. By specifying the buckling load and frequency, the variation of young modulus was obtained along the axial direction of the beam. Li and Batra [109] developed analytical relationship between critical buckling loads of FG Timoshenko beam and their corresponding homogenous EBBT under compressive load for specific boundary conditions. Rahimi et al. [110] studied the buckling of FG beams using an exact solution based on TBT, incorporating nonlinear strain-displacement relations and the effects of shear strain and rotary inertia. Nguyen et al. [111] introduced a FSDT for investigating buckling, vibration, and bending behaviors of FG beams, deriving an enhanced shear stiffness formulation and SCF using analytical solution. Huang et al. [112] carried out the buckling behavior of axially FG and non-uniform Timoshenko beams using a, approach based on auxiliary functions and power series. A system of linear algebraic equations is used to determine the critical buckling loads under various boundary conditions. Trinh et al. [113] presented an exact solution to analyze buckling and vibration behaviors of FG beams subjected to mechanical and thermal loads, considering different boundary conditions. Şimşek [114] analyzed the buckling behavior of 2D FGM beams , with properties varying in both thickness and axial directions according to power-law. Based on TBT the critical buckling load is obtained utilizing Ritz method. Sayyad and Ghugal [115] proposed a modified ESDT for evaluate buckling, bending, and free vibration of FG beams. This theory captures higher-order variation of shear stress across the depth, while satisfying traction-free conditions, without requiring SCF.

Kahya and Turan [116] introduced FE model for analyzing Buckling and free vibration response of FG beams. The governing equation were obtained using Lagrangian relationships. A refined zigzag theory (RZT) was developed by Farhatnia and Sarami [117] based on FEM to study buckling and static behavior of thick FG beams. Unlike layerwise theories, the proposed model doesn't need SCF and the number of the variables is independent of the number of layers. Carrera and Demirbas [118] carried out the nonlinear bending and buckling of 1D FG beams utilizing CUF combined with Lagrangian Extension (LE) and the material properties were assumed to vary exponentially. Demirhan [49] studied the buckling behavior of FG Timoshenko beam under various boundary conditions. This study examines the influence of various parameters and boundary conditions on the critical buckling load.

Eslami et al. [119] carried out thermal buckling of FG beams , deriving the equilibrium and stability equations using 1D elasticity theory. A close form solution for critical thermal loads are obtained for beams with six different boundary conditions. Kiani and Eslami [120] investigated the buckling response of FGM beams under different thermal loading types using an analytical solution. The analysis is based on EBBT with material properties varying across the thickness according to the power law. Wattanasakulpong et al. [121] employed an enhanced TSDT to analyze thermal buckling and vibration of FG beams, using the Ritz method to solve the problem. Kiani and Eslami [122] analyzed the buckling behavior of FGM beams using TBT under thermomechanical loading, considering temperature-depending. Closed-form solution for critical temperature were derived for diverse boundary conditions. She et al. [123] focused on predicting thermal buckling of FGM beams employing different beam theories. the analysis considers for temperature depending properties under uniform temperature rise. A two-step perturbation method is utilized to evaluate critical temperature of FGM beam with clamped ends. Alimoradzadeh et al. [124] analyzed the thermal buckling temperature and nonlinear vibration of FG fiber reinforced beam, using EBBT and accounting for Von Karman geometrical nonlinearity. The nonlinear differential equations are discretized using Galerkin method and solved analytically for three different boundary conditions. Gayen [125] carried out an analytical method to study thermo-elastic buckling and vibration response of FG beams using various gradation laws. The material properties are temperature-depending, and the equations of motions are determined using Hamilton principle. To understand the impact of geometric and temperature parameters on thermo-elastic buckling and vibration a parametric study is conducted.

Nguyen et al. [126] introduced a new HSDT for analyzing buckling and vibration behavior of FG sandwich beams, featuring a hyperbolic distribution of shear strain. They also developed new quasi-3D [127] with hyperbolic displacement to investigate the mechanical behaviors of sandwich beams. Nguyen and Nguyen [128] proposed an advanced TSDT incorporating trigonometric function for analyzing buckling, static, and free vibration of FG sandwich beams. Bennai et al. [129] presented a HSDBT explores dynamic and buckling response FG sandwich beams, considering both shear and normal strain.

Vo et al. [130] carried out a FE employing RSDT to evaluate the stability and dynamic behaviors of sandwich beams with FG faces. The mathematical framework, derived through Hamilton principle establishes equations of motion. A new FE based FSDT was introduced by Kahya and Turan [131] to analyze buckling and vibration of FG sandwich beams, featuring 3N+7 DOFs per N-layer. This research two different sandwich configurations. The model performance was confirmed through comparative studies. Fazzolari [132] studied the buckling and vibration behavior of 3D FG sandwich beams with dual porosity, supported by the Winkler-Pasternak foundation and different boundary conditions. The analysis was done using various beam theories. Al-shujairi and Mollamahmutoğlu [133] used nonlocal strain theory and multiple HSDTs to examine the stability and free vibrations behavior of FG micro-beams, incorporating thermal effect elastic foundation support. This research provides novel insight into how structure responses are affected by various parameters including nonlocal effects, material gradients, geometric configurations, and foundation properties. Liu et al. [134] investigated the thermomechanical buckling of clamped porous FG sandwich beams, utilizing SSDT and modified Voigt law to analyze temperature-depending properties and porosity effect. The study examines various thermal conditions while considering the physical neutral plane. The obtained results are validated against ABAQUS simulations. Ellali et al. [135] examinate the thermal stability of FG sandwich beams with integrated piezoelectric layers using TSDT, considering the combined effect of thermal loading and constant voltage. The research reveals how critical buckling is influenced by multiple factors, thermal loading type, and piezoelectric voltages.

It can be seen in literature motioned above that many manuscripts have conducted on vibrations analysis of FG and sandwich beams [92, 94, 97, 99, 107, 108, 110, 111, 113, 115, 116, 121, 125-128, 130-133]. The following section presents more research on the vibration analysis of FGM beams.

2.5.3. Vibration analysis

The analysis of functionally graded beams has been a subject of comprehensive investigation. A numerous of studies have been devoted to establishing exact solutions for examining the vibration of FG beams. Aydogdu and Taskin [136] explored the vibration behavior FG beams, examining the structure with both exponential and power laws variations of Young modulus through their depth. The study employs multiple theoretical approaches, with frequencies determined through Navier's solution based on equations derived from Hamilton principle. Sina et al. [137] proposed a novel beam theory explores the vibrational behavior of FGM beams, where material properties change along the depth according to the power law. Using Hamilton principle and assume zero lateral stress to develop motion equations, which are solved analytically. Chehel Amirani et al. [138] examined the free vibration of sandwich beams using FGM as core, implementing element free Galerkin method and 2D elasticity formulation. The investigation derives first ten natural frequencies of the sandwich beam. Ait Atmane et al. [139] examines the free vibration of E-FGM beam. Employing an analytical method, the study derives solutions for natural frequencies across different boundary conditions. The analysis of Free vibration of FG beams was conducted by Koochaki [140] using Reddy's TSDT, to study simply supported FG beams, employing the Navier solution. Thai and Vo [141] investigation focused on analyzing the vibration and bending of FG beams through multiple HSDTs. The research provides analytical solutions and examines how the power law index and shear strain impact the beam's behaviors. Akbaş [142] analyzed the vibration and bending of FG beam supported by a Winkler foundation, using EBBT and TBT. The authors developed an exact solution for deflection and frequencies utilizing the minimum potential energy and Navier approach. Hadji et al. [143] introduced a new FSDT to evaluate the FG beam's dynamic response. The proposed model generates governing equations for axial and transverse deformation, maintaining mathematical simplicity while accounting for material gradation effects. Wang et al. [144] presented a mathematical study explores the vibration of FG beams, utilizing an exact solution for natural frequencies in different beam support conditions. Through the application of Levinson beam theory Wang and Li [145] developed analytical solutions addressing free vibration and bending behaviors of FGM beams. Their analysis explores how volume fraction and boundary conditions influence the vibration response. Yildirim [146] explored vibration of sandwich beams with FG core, utilizing plane stress conditions and 2D elasticity formulation.

Doroushi et al. [147] studied both forced and free vibration of FG piezoelectric beam subjected to combined thermal, electric, and mechanical forces using HSDT, the problem solved using FEM. Utilizing FEM, Alshorbagy et al. [148] conducted an analysis of dynamic behavior in functionally graded beams. By using virtual work principle and CBT the equations of motions were obtained. The investigation examined how different parameters effects the beam's vibrational behavior. Taeprasartsit [149] developed mathematical framework to analyze large amplitude vibrations in thin FG beams with fixed ends, employing FEM based on EBBT an Von Karman nonlinearity. A novel high-order element using an integrated TBT is developed by Katili et al. [150], featuring a two-node element with Hermitian functions that prevents shear locking while incorporating shear effects. The proposed model is applied to analyze the static and vibrational behaviors of FG beams. Belarbi et al. [151] carried out free vibration response in both symmetric and asymmetric FG sandwich beams, applying Hermite-Lagrangian FEM based on HSDBT, featuring three variables and eliminating the necessity of SCF.

Su et al. [152] analyzed free vibration and buckling of FG sandwich beams with various boundary conditions and Pasternak foundation support, using a modified Fourier series that incorporates both cosine and supplemented functions. Bouakkaz et al. [153] introduced a hyperbolic model to analyze free vibration response of FG sandwich beams, employing Hamilton principle. The influence of volume fraction geometrical configuration, and boundary condition on critical buckling load and free vibration were explored. Trinh et al. [154] presented analytical solution for evaluating fundamental frequencies of FG sandwich beams, incorporating CBT, FSDT, and HSDTs.

Mashat et al. [155] conducted an investigation of natural frequencies in FG sandwich beams, using multiple theories and FE based on CUF. A study by Tossapanon and

Wattanasakulpong [156] investigated the stability and dynamic behaviors of FG sandwich beams supported by dual- parameter elastic foundation. Bouamama et al. [157] analyzed the vibrational behavior of FG sandwich beams under diverse boundary conditions, with particular focus on how the skin depth effects on the beam frequencies. Akbas [158] examined forced vibration response of deep sandwich beams with porose core and FG Faces, subjected to harmonic loads.

A computational investigation utilizing FEM was performed by Bhangale and Ganesan [159] to understand the thermal influence on vibration and stability behaviors of clamped FG sandwich beams. Pradhan and Murmu [160] studied the thermo-mechanical vibration of FG and sandwich beams supported by Winkler Foundations, using modified differential quadrature method (DQM) with Chebyshev functions. The effect of temperature type, volume fraction, and foundation characteristic are examined.

Rahmani and Dehghanpour [161] carried out the vibration analysis in two sandwich configurations, one with FG coating over an isotropic core, and another one with isotropic outer layers around an FG core. The analysis employs an enhanced beam theory incorporating core flexibility, various porosity distribution, temperature depending properties, utilizing Galerkin method and Hamilton principle for mathematical modeling. Zhang et al. [162] analyzed the nonlinear vibration of FG sandwich beam featuring pyramidal truss core and FG layers subjected to thermomechanical loads. The authors developed a model to calculate shear modulus of the core under non-uniform temperature loads Li et al. [163] carried out the thermal vibration of FG sandwich beams, employing nonlinear FE simulation. The results demonstrate that the beams with auxetic core exhibit superior performance.

2.6. Conclusion

This chapter introduces fundamental beam theories used for analyzing FGM beams. Classic beam theory, being the earliest and most straightforward approach, primarily address thin beams behaviors while overlooking shear stress effects. Timoshenko beam theory assumes uniform displacement along beam thickness. It predicts constant shear strain, although actual shear strain distribution is quadratic. To precisely represent the stress, we must implement a correction factor. Higher-order shear deformation theories expand the displacement field using more variations relative to the thickness. These approaches offers more accurate representation of beam's mechanical behaviors compared simpler theorical frameworks.   An overview of scientific literature is presented, focusing on the mechanical and thermal response of functionally graded and sandwich beams. The research encompasses multiple analytical and numerical solutions developed to investigate the static, buckling vibration behaviors.

Part II Development of new finite element model based on enhanced Timoshenko beam theory

Chapter 3:

Development of enhanced Timoshenko beam theory (ETBT)

3.1. Introduction

This chapter introduces a new high-order shear deformation model, based on enhanced Timoshenko theory (ETBT), for analyzing the behavior of FG and sandwich beams. The proposed model utilizes only three unknowns and incorporates a quadratic variation of shear strain across the beam thickness. It satisfies the zero shear-stress condition at both the upper and the lower surfaces of the beam without requiring a correction factor.

Based on this model, a beam element has been developed to perform static, buckling, and free vibration analysis of Functionally graded material beams, considering both thermal and non-thermal effects. The formulated element consists of two nodes, each possessing three degrees of freedom. Material properties are assumed to vary through the thickness following a power law distribution, expressed in terms of the constituent volume fraction.

The stiffness, geometric, and mass matrices are formulated using the principle of total potential energy, Euler-Lagrange equation, and Hamilton principle. Additionally, the concept of the physical neutral axis is employed to avoid stretching-bending phenomenon.

3.2. A new high order shear deformation theory

This chapter, presents a new high-order shear deformation theory. This model enhances Timoshenko theory by accounting for the influence of stretching.

3.2.1. Displacement field

The proposed displacement field for the beam is assumed to be [164]:

$$\begin{aligned} u(x,z,t) &= u_0 + z\varphi_x \\ w(x,z,t) &= w_0 + z^2\psi_z \end{aligned} \tag{3.1}$$

In this context, u and v represent the displacement of a point R (x, z) within the beam. The terms u_0 and v_0 refer to the displacement components of the central axis along the x and z directions, respectively. φ_x denotes the rotation, ψ_z indicates the stretching contribution.

3.2.2. Kinematics

Introducing Von Karman nonlinear relationship [165], the strain components associated with the proposed displacement field are expressed as:

$$\varepsilon_x = \varepsilon_x^0 + zk_x + \varepsilon^{nl} \tag{3.2}$$

$$\gamma_{xz} = \gamma_{xz}^0 + z^2\psi_z^0 \tag{3.3}$$

Where

$$\varepsilon_x^0 = \frac{\partial u_0}{\partial x} \tag{3.4}$$

$$k_x = \frac{\partial \varphi_x}{\partial x} \tag{3.5}$$

$$\gamma_{xz}^0 = \frac{\partial w_0}{\partial x} + \varphi_x \tag{3.6}$$

$$\varepsilon^{nl} = \frac{1}{2}\left(\frac{dw}{dx}\right)^2 \tag{3.7}$$

ε_x^0 : axial strain

k_x : curvature

γ_{xz}^0 : shear strain

ε^{nl} : nonlinear strain

Using shear stress-free boundary condition on the top and bottom of the beam.

$$\gamma_{xz}\left(\pm\frac{h}{2}\right) = \gamma_{xz}^0 + \frac{h^2}{4}\psi_z^0(x) = 0 \tag{3.8}$$

Which lead to

$$\psi_z^0 = -\frac{4}{h^2}\gamma_{xz}^0 \tag{3.9}$$

By introducing Eq (3.9) into Eq (3.3), the shear strain relationship can be formulated as:

$$\gamma_{xz} = \Gamma_1 \gamma_{xz}^0 \tag{3.10}$$

Γ_1 is shear function defined by:

$$\Gamma_1(z) = \left(1 - 4\frac{z^2}{h^2}\right) \tag{3.11}$$

- **Shear function improvement**

Shear correction factor is used in Timoshenko theory to consider the supposition of uniform shear strain across the thickness of the beam. This factor is calculated by comparing shear strain energy from elasticity theory with that predicted by Timoshenko theory. Consequently, the shear stress for an isotropic material is written as:

$$\sigma_{xz} = \frac{5}{6}\gamma_{xz}^0 Q \tag{3.12}$$

$$Q = \frac{1}{2(1+\upsilon)}E \tag{3.13}$$

Q represent the stiffness coefficient, and *E* stands for young's modulus.

Timoshenko's shear strain energy per unit of area is given by:

$$U_{ss}^{TM} = \frac{1}{2}\int_{\frac{-h}{2}}^{\frac{h}{2}} \sigma_{xz}\gamma_{xz} dz \tag{3.14}$$

By substitution the expression from Eq (3.12) into Eq (3.14) and preforming integration through the depth, we can reformulate Eq (3.14) as follows:

$$U_{ss}^{TM} = \frac{5}{12}Qh\left(\gamma_{xz}^0\right)^2 \tag{3.15}$$

When shear strain exhibits quadratic variation along the thickness, the shear stress may be expressed as:

$$\sigma_{xz} = \Gamma(z)Q\gamma_{xz} \tag{3.16}$$

$$\Gamma(z) = C\left(1 - \frac{4z^2}{h^2}\right) \tag{3.17}$$

$\Gamma(z)$ represent enhanced shear function, and *C* is Constant.

The shear strain energy per unit of area can be formulated as:

$$U_{ss}^{\Gamma} = \frac{1}{2}\int_{\frac{-h}{2}}^{\frac{h}{2}} \sigma_{xz}\gamma_{xz}dz = \frac{1}{2}\int_{\frac{-h}{2}}^{\frac{h}{2}} Q\left(\Gamma(z)\right)^2 \left(\gamma_{xz}^{0}\right)^2 dz \tag{3.18}$$

Performing thickness integration on Eq (3.18) yields:

$$U_{ss}^{\Gamma} = \frac{4h}{15} Q\left(\gamma_{xz}^{0}\right)^2 C^2 \tag{3.19}$$

The value of the constant C is determined by setting Eq (3.15) equal to Eq (3.19)

$$C = \frac{5}{4} \tag{3.20}$$

Based on the preceding analysis, we can recast the displacement field in this way

$$\begin{aligned} u(x,z,t) &= u_0 + z\varphi_x \\ w(x,z,t) &= \Gamma(z)w_0 + \left(\Gamma(z) - 1\right)G(x) \end{aligned} \tag{3.21}$$

Where

$$\Gamma(z) = \frac{5}{4}\left(1 - \frac{4z^2}{h^2}\right) \tag{3.22}$$

$$\varphi_x = \frac{dG(x)}{dx} \tag{3.23}$$

The strain relations may be restated as follows:

$$\varepsilon_x = \varepsilon_x^0 + zk_x + \varepsilon^{nl} \tag{3.24}$$

$$\gamma_{xz} = \Gamma(z)\gamma_{xz}^{0} \tag{3.25}$$

3.3. Governing Equations

3.3.1. Material properties

A FGM beam with rectangular geometry is considered. The beam is defined by length ***L*** and cross-sectional area with a thickness ***h*** and width ***b*** (Figure 3.1). In this study, the Poisson's ratio ***v*** is maintained as a constant for simplification. Conversely, other material properties, including Young's modulus ***E***, thermal expansion ***α***, and mass density ***ρ***, are posited to exhibit continuous variation across the thickness according to the power law. These properties can be mathematically described as [166]:

$$\begin{aligned} E(z) &= E_m + \left(E_c - E_m\right)V_c \\ \alpha(z) &= \alpha_m + \left(\alpha_c - \alpha_m\right)V_c \\ \rho(z) &= \rho_m + \left(\rho_c - \rho_m\right)V_c \end{aligned} \tag{3.26}$$

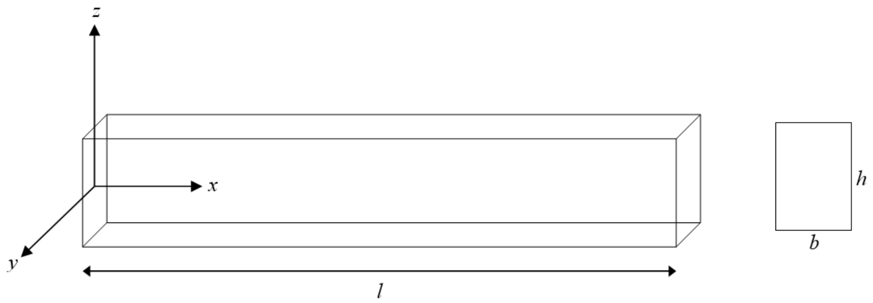

Figure 3.1 FGM beam geometry and coordinate

The subscripts ***c*** and ***m*** denote the ceramic and metallic materials respectively, while $\boldsymbol{V_c}$ represent the volume fraction.
In this study two types of FGM beams are considered: (A) FG beam; and sandwich beam

- **FG beam**

This beam is graded from metal to ceramic (Figure 3.2) with volume fraction V_c written as follows:

$$V_c = \left(\frac{1}{2} + \frac{z}{h}\right)^p, \qquad \mathrm{z} \in \left[-\frac{h}{2}, \frac{h}{2}\right] \tag{3.27}$$

p denotes power-law index

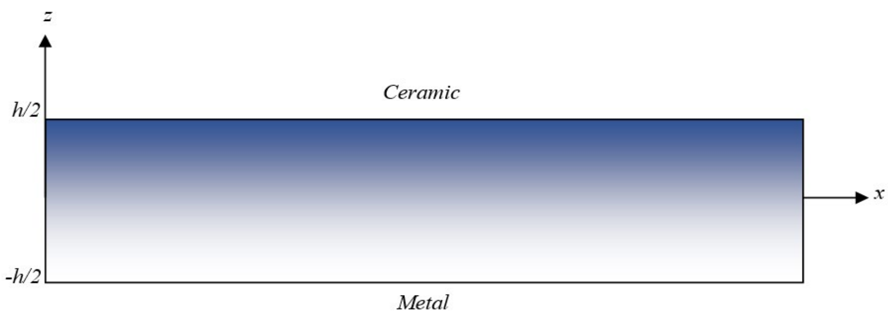

Figure 3.2 Functionally Graded beam

- **Sandwich beam**

The upper and lower layers of the sandwich beams consist of FGM, while the core layer is composed of ceramic or metallic as shown in figure 3.3. The volume fraction V_c is defined by:

$$\begin{cases} V_c = \dfrac{h_2 + \dfrac{h_1}{2} - z}{h_2}, & z \in \left[\dfrac{h_1}{2} \le z \le h_2 + \dfrac{h_1}{2}\right] \quad \text{(Top layer)} \\ V_c = 1, & z \in \left[-\dfrac{h_1}{2} \le z \le \dfrac{h_1}{2}\right] \quad \text{(Core)} \\ V_c = \dfrac{h_0 + \dfrac{h_1}{2} + z}{h_0}, & z \in \left[-h_0 - \dfrac{h_1}{2} \le z \le \dfrac{h_1}{2}\right] \quad \text{(Bottom layer)} \end{cases} \tag{3.28}$$

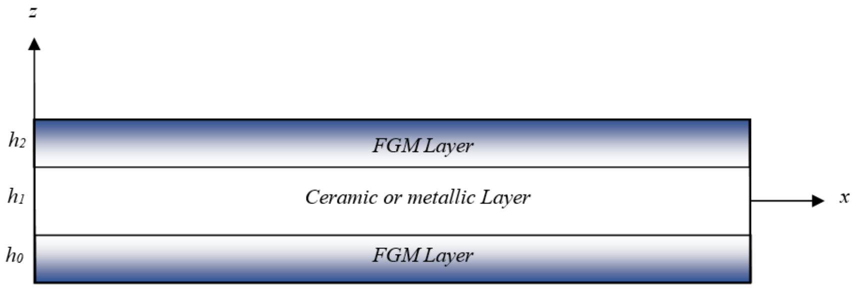

Figure 3.3 Sandwich beam with FGM skin and homogeneous core

3.3.2. Constitutive equations

For an elastic FG beam, the stress-deformation relationship may be written as:

$$\begin{aligned} \sigma_x &= E(z)(\varepsilon_x - \varepsilon_T) \\ \sigma_{xz} &= Q\gamma_{xz} \end{aligned} \tag{3.29}$$

ε_T denotes strain due temperature rise, which can be expressed by:

$$\varepsilon_T = \alpha(z)\Delta T \tag{3.30}$$

3.3.3. Physical neutral axis

The heterogeneous distribution of material properties in the beam results in a coupled stretching-bending behavior. To simplify the analysis, force and moment resultant are evaluated with respect to the physical neutral axis. Which deviates from the beam's centroidal axis, as illustrated in Figure 3.4. Calculating the location of physical neutral axis needs determining the value e, at which the axial force induced by bending becomes zero [165, 167]. This be expressed through the following equation:

$$z_{na} = z - e \tag{3.31}$$

where e is the distance between the neutral axis and the centroid of the beam

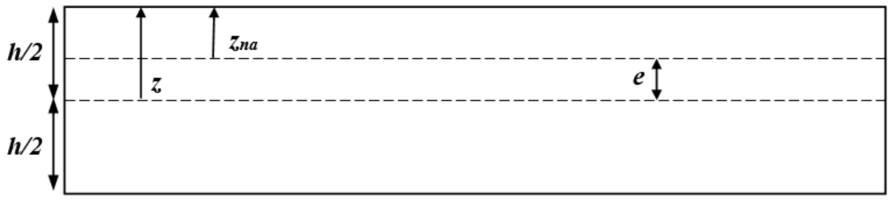

Figure 3.4 Physical neutral axis position

e is determined by setting the axial force due bending to zero at the point where $y = e$ [72]

$$\int_{-\frac{h}{2}}^{\frac{h}{2}} \sigma_x dz = \int_{-\frac{h}{2}}^{\frac{h}{2}} E(z)\left(z-e\right)\frac{d\varphi_x}{dx}dz = 0 \tag{3.32}$$

Through simplification of Eq (3.32), we obtain:

$$\int_{-\frac{h}{2}}^{\frac{h}{2}} E(z)(z-e)dz = \int_{-\frac{h}{2}}^{\frac{h}{2}} E(z)z - e\int_{-\frac{h}{2}}^{\frac{h}{2}} E(z)dy = 0 \tag{3.33}$$

So, the neutral axis position can be calculated using the following relation:

$$e = \frac{\int_{-\frac{h}{2}}^{\frac{h}{2}} E(z)zdz}{\int_{-\frac{h}{2}}^{\frac{h}{2}} E(z)dz} \tag{3.34}$$

3.3.4. Forces and moments

The forces and moment resultant are determined by integrating the respective stress across the thickness, as written in the following equations:

$$N_x = \int_{-\frac{h}{2}}^{\frac{h}{2}} \sigma_x dz \tag{3.35}$$

$$M_x = \int_{-\frac{h}{2}}^{\frac{h}{2}} \sigma_x z_{na} dz \tag{3.36}$$

$$S_{xz} = \int_{-\frac{h}{2}}^{\frac{h}{2}} \sigma_{xz} dz \tag{3.37}$$

The correlation between the stress resultants and deformations is given as:

$$\begin{Bmatrix} N_x \\ M_x \\ S_{xz} \end{Bmatrix} = \begin{bmatrix} A & 0 & 0 \\ 0 & D & 0 \\ 0 & 0 & H \end{bmatrix} \begin{Bmatrix} \varepsilon_x^0 \\ k_x \\ \gamma_{xz} \end{Bmatrix} \tag{3.38}$$

The terms A, D, and H represent the elastic coefficient, these coefficients are written mathematically as follows:

$$\{A \quad D \quad H\} = \int_S E(z) \times \left\{1 \quad (z-e)^2 \quad \Gamma(z)\mathrm{Q}\right\} dS \tag{3.39}$$

3.4. Finite element formulation

To analyze the static, buckling, and free vibration of FG and sandwich beams, both with and without thermal effect, a two-node finite element is used. This element is based on an improved Timoshenko theory and features three degrees of freedom (DOFs) per node.

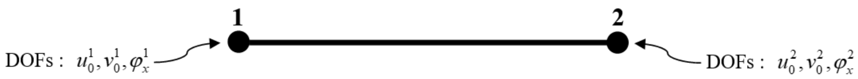

Figure 3.5 finite element of ETBT

3.4.1. Displacement interpolation

The present finite element's displacement field is defined by:

$$\theta_\alpha(x) = \sum_{i=1}^{2} N_i \theta_\alpha^i, \quad \alpha=1,2,3 \tag{3.40}$$

Where $\theta_\alpha^i = u_0^i, w_0^i, \varphi_x^i, \quad i = 1,2$

θ_α represent the displacement or rotation at an arbitrary point of the element. The terms N_i and θ_α^i are the Lagrange shape function and displacement component associated with node *i*, respectively.

Lagrange shape functions are represented by the following formula:

$$N_1 = 1 - \frac{x}{L}$$
$$N_2 = \frac{x}{L} \tag{3.41}$$

3.4.2. Strain displacement relations

By employing shape functions, the strain-displacement relations expressed in Eqs (3.4)-(3.7) can be rewritten as:

$$\varepsilon_x^0 = \left[B_a\right]\left\{q\right\} \tag{3.42}$$

$$k_x = \left[B_b\right]\left\{q\right\} \tag{3.43}$$

$$\gamma_{xz}^0 = \left[B_s\right]\left\{q\right\} \tag{3.44}$$

$$\frac{dw}{dx} = \left[G\right]\left\{q\right\} \tag{3.45}$$

The matrices $\left[B_a\right], \left[B_b\right], \left[B_s\right]$ and $\left[G\right]$ are of dimension (1×6), where the subscripts *a*, *b*, and *s* denote the axial, bending, and shear strain, respectively. $\left\{q\right\}$ represent displacement vector.

These matrices can be derived from the shape function as follows:

$$\left[B_a\right] = \begin{bmatrix} \frac{\partial N_i}{\partial x} & 0 & 0 \end{bmatrix} \quad \left(i = 1,2\right) \tag{3.46}$$

$$\left[B_b\right] = \begin{bmatrix} 0 & 0 & \frac{\partial N_i}{\partial x} \end{bmatrix} \quad \left(i = 1,2\right) \tag{3.47}$$

$$\left[B_s\right] = \begin{bmatrix} 0 & \frac{\partial N_i}{\partial x} & N_i \end{bmatrix} \quad \left(i = 1,2\right) \tag{3.48}$$

$$\left[G\right] = \begin{bmatrix} 0 & 0 & \frac{\partial N_i}{\partial x} \end{bmatrix} \quad \left(i = 1,2\right) \tag{3.49}$$

$$\left\{q\right\}^T = \left\{u_0^i \quad w_0^i \quad \varphi_x^i\right\} \quad \left(i = 1,2\right) \tag{3.50}$$

3.4.3. Derivation of elementary matrices

The elementary stiffness and geometric matrices of the element are derived using the total potential energy, which is defined as:

$$\Pi = U + W \tag{3.51}$$

with U being the strain energy and W the potential energy of external loads.

The strain energy of beam is expressed as:

$$\begin{aligned} U &= \frac{1}{2}\int_V \left(\left\{ \varepsilon^l \right\}^T \sigma_x + \left\{ \gamma_{xz} \right\}^T \sigma_{xz} \right) dV \\ &= \frac{1}{2}\int_\Omega \int_{-\frac{h}{2}}^{\frac{h}{2}} \left(\left\{ \varepsilon_x^0 \right\}^T \sigma_x + z_{na} \left\{ k_x \right\} \sigma_x + \left\{ \gamma_{xz} \right\}^T \sigma_{xz} \right) d\Omega dz \end{aligned} \tag{3.52}$$

Ω denote the beam's surface.

Substitution Eqs (3.35), (3.36), and (3.37) into Eq (3.52), the strain energy may be rewritten as:

$$U = \frac{1}{2}\int_\Omega \left(\left\{ \varepsilon_x^0 \right\}^T N_x + \left\{ k_x \right\}^T M_x + \left\{ \gamma_{xz} \right\}^T S_{xz} \right) d\Omega \tag{3.53}$$

Using Eq (3.38), Eq (3.53) can be reformulated as follows:

$$U = \frac{1}{2}\int_0^l \left(\left\{ \varepsilon_x^0 \right\}^T [A] \left\{ \varepsilon_x^0 \right\} + \left\{ k_x \right\}^T [D] \left\{ k_x \right\} + \left\{ \gamma_{xz} \right\}^T [H] \left\{ \gamma_{xz} \right\} \right) dx \tag{3.54}$$

Introducing the strain-displacement relationships defined in Eqs (3.42), (3.43), and (3.44) into the preceding expression yields:

$$U = \frac{1}{2}\int_0^l \left(\{q\}^T \left([B_a]^T A [B_a] + [B_b]^T D [B_b] + [B_s]^T H [B_s] \right) \{q\} \right) dx \tag{3.55}$$

3.4.3.1. Static analysis

The external work performed by the distributed load *F(x)* on the beam is expressed by the following formula:

$$\begin{aligned} W &= \int_0^l F(x) w_0(x) dx \\ &= \int_0^l F(x) \{q\}^T [N]^T dx \end{aligned} \tag{3.56}$$

By substitution of Eqs (3.55) and (3.56) into (3.51) leads to the following expression:

$$\begin{aligned} \Pi = {} & \frac{1}{2}\int_0^l \left(\{q\}^T \left([B_a]^T A [B_a] + [B_b]^T D [B_b] + [B_s]^T H [B_s] \right) \{q\} \right) dx \\ & -\int_0^L F(x) \{q\}^T [N] dx \end{aligned} \tag{3.57}$$

Setting the first variation of the total potential energy with respect to the nodal value q to zero yields the following equilibrium equation:

$$[K_e]\{q\} = \{F_e\} \tag{3.58}$$

$$[K_e] = \int_0^l \left(\underbrace{[B_a]^T A [B_a]}_{axial} + \underbrace{[B_b]^T D [B_b]}_{bending} + \underbrace{[B_s]^T H [B_s]}_{shear} \right) dx \tag{3.59}$$

$$\{F_e\} = \int_0^l F(x)[N]^T\, dx \tag{3.60}$$

$$[N] = [0 \quad N_1 \quad 0 \quad 0 \quad N_2 \quad 0] \tag{3.61}$$

$[K_e]$: Elementary stiffness matrix.

$\{F_e\}$: Nodal load vector.

$[N]$: Shape functions matrix.

3.4.3.2. Buckling analysis

The potential energy of external loads, resulting from either thermal or mechanical forces, is given by:

$$W = \frac{1}{2}\int_0^l \{\varepsilon^{nl}\} P dx \tag{3.62}$$

By substitution Eqs (3.7), (3.45), (3.55), and (3.62) in the total potential energy principle yields:

$$\begin{aligned} \Pi = &\frac{1}{2}\int_0^l \left(\{q\}^T \left([B_a]^T A [B_a] + [B_b]^T D [B_b] + [B_s]^T H [B_s] \right) \{q\} \right) dx \\ &+ \frac{1}{2}\int_0^l \{q\}^T [G]^T P [G] \{q\}\, dx \end{aligned} \tag{3.63}$$

Eliminating the second variation of the total potential energy with respect to nodal values leads to the following eigenvalue problem:

$$\left([K_e] + [K_e^g] \right) \{q\} = 0 \tag{3.64}$$

$[K_e^g]$ represent geometric matrix

$$[K_e^g] = \int_0^l [G]^T P [G] dx \tag{3.65}$$

The introduction of loading factor λ allow us to rewrite the stress as: $P = \lambda P_0$.

P_0 denotes the stress due the mechanical load or temperature rise ΔT_0.

$$\left[K_{e0}^{g}\right]=\int_{0}^{l}\left[G\right]^{T}P_{0}\left[G\right]dx \tag{3.66}$$

The eigenvalue problem for calculating the critical buckling is given by:

$$Det\left(\left[K_{e}\right]+\lambda\left[K_{e0}^{g}\right]\right)=0 \tag{3.67}$$

3.4.3.3. Free vibration analysis

Hamilton's principle can be used to derive the governing equations for free vibration problems, which is defined by:

$$\delta\int_{t_1}^{t_2}Ldt=0 \tag{3.68}$$

L represent Lagrangian of the system, expressed as $L=T-\Pi$, where T denote the kinetic energy and Π is the potential energy. t_1 and t_2 are initial and the final instant. Therefore, Hamilton principle can be rewritten as:

$$\begin{aligned}&\delta\int_{t_1}^{t_2}\left(T-\Pi\right)dt=0\\&\delta\int_{t_1}^{t_2}\left(T-\left(U+V\right)\right)dt=0\end{aligned} \tag{3.69}$$

While

$$T=\frac{1}{2}\int_{\Omega}\int_{-\frac{h}{2}}^{\frac{h}{2}}\rho(z)\left(\dot{u}^{2}+\dot{w}^{2}\right)dzd\Omega \tag{3.70}$$

Where $\dot{u}=\frac{du}{dt}$ and $\dot{w}=\frac{dw}{dt}$

The time variation of kinetic energy may be expressed as:

$$\delta T=\int_{\Omega}\int_{-\frac{h}{2}}^{\frac{h}{2}}\rho(z)\left(\ddot{u}\delta u+\ddot{w}\delta w\right)dzd\Omega \tag{3.71}$$

Integrating Eq (3.71) over the thickness yields the following expression:

$$\delta T=\int_{\Omega}\left(I_{0}\left(\ddot{u}_{0}\delta u_{0}+\ddot{w}_{0}\delta w_{0}\right)+I_{2}\left(\ddot{\varphi}_{x}\delta\varphi_{x}\right)\right)d\Omega \tag{3.72}$$

$(\ddot{\ })$ denote the second derivative with respect to time. I_0 and I_2 represent the moment of inertia, defined as follows:

$$I_0, I_2 = \int_{-\frac{h}{2}}^{\frac{h}{2}} \rho(z)\left(1, (z-e)^2\right) dz \tag{3.73}$$

By employing Euler-Lagrange equation, as expressed below:

$$\frac{d}{dt}\left(\frac{\partial L}{\partial \dot{q}}\right) - \frac{\partial L}{\partial q} = 0 \tag{3.74}$$

It leads to the following equation of motion:

$$\left[M\right]\{\ddot{q}\} + \left[K\right]\{q\} = 0 \tag{3.75}$$

$$\left[M\right] = \int_0^l \left[N\right]^T \left[I\right]\left[N\right] dx \tag{3.76}$$

$$\left[K\right] = \left[K_e\right] + \left[K_e^g\right] \tag{3.77}$$

$\left[M\right]$ represents the mass matrix. $\left[N\right]$ and $\left[I\right]$ are the shape function and inertia matrices, respectively, and they defined as follows:

$$\left[N\right] = \begin{bmatrix} N_1 & 0 & 0 & N_2 & 0 & 0 \\ 0 & N_1 & 0 & 0 & N_2 & 0 \\ 0 & 0 & N_1 & 0 & 0 & N_2 \end{bmatrix} \tag{3.78}$$

$$\left[I\right] = \begin{bmatrix} I_0 & 0 & 0 \\ 0 & I_0 & 0 \\ 0 & 0 & I_2 \end{bmatrix} \tag{3.79}$$

Substituting $\left\{\ddot{q}\right\} = -\omega^2 \left\{q\right\}$ into the equation of motion, we obtain:

$$\left(\left[K\right] - \omega^2 \left[M\right]\right)\{q\} = 0 \tag{3.80}$$

3.5. Conclusion

This chapter presented a new high-order shear deformation model with three unknowns for analyzing FGM beams. This model incorporates a quadratic variation of shear stress through the thickness, ensuring zero shear stress at the top and bottom surfaces of the beam, eliminating the need for a shear correction factor. Based on this model, a two-node finite element is formulated with three DOFs per node. This element is employed for static, buckling, and free vibration analyses of FG and sandwich beams with and without thermal effects. The material properties of the beams follow a power-law distribution across the thickness. To prevent the stretching-bending coupling effect arising from the beam's asymmetry, force and moment resultants are determined with respect to the physical neutral axis, which is distinct from the beam's centroid. The stiffness, geometric, and mass matrices are derived using the principles of total potential energy, Hamilton's principle, and the Euler-Lagrange equation.

Chapter 4:
Application ETBT on FG beams-Results and discussions

4.1. Introduction

This chapter presents numerical analysis to evaluate the capabilities of developed model (ETBT). The analysis examines the convergence, computational accuracy, and numerical stability. The investigation addresses different response of functionally graded beams, including static, mechanical, thermal buckling, and free vibration behaviors. The model validation is achieved through a comparison with previously published research results, while investigating how various parameters affect the FG beam behaviors.

4.2. Functionally graded beams analysis

This section presents the static, buckling, and free vibration of FG beams under mechanical and thermal loads. The analysis were conducted by examining diverse material composition. The detailed material properties utilized through this investigation are presented in Table 4.1:

Table 4.1 Material properties of FG beams [113]

	Properties	E (MPa)	ρ (Kg/m^3)	υ	α (1/K)
Top	Alumina (Al_2O_3)	380	3960	0.3	$8.4e^{-6}$
surface	Silicon nitride (Si_3N_4)	322.27	-	0.3	$7.4746e^{-6}$
Bottom	Aluminum (Al)	70	2702	0.3	$23.1e^{-6}$
surface	Stainless steel (SUS304)	207.79	-	0.3	$15.32e^{-6}$

Three distinct supports were used to evaluate FGM beams response:

- Simply Supported (S-S)
- Clamped-Clamped (C-C)
- Clamped-Free (C-F)

To ensure the accuracy and validate the present model, the beam was segmented into multiple elements, specifically utilizing mesh configurations of 50, 100, 150, 200, and 250 elements

4.3. Static Analysis of FG beams

To validate the developed model's reliability, initial assessments focused on evaluating the static response of Alumina-Aluminum FG beams with length-to-thickness ratio (L/h=5, 10) and different ends support under uniform distributed load (UDL) q_0. the numerical results are expressed through dimensionless parameters for displacement and stresses, calculated using the following relationships:

$$\begin{aligned}
&\overline{w} = \begin{cases} \dfrac{100E_m h^3}{L^4 q_0} w\left(\dfrac{L}{2}\right) & \text{S-S , C-C} \\ \dfrac{100E_m h^3}{L^4 q_0} w(L) & \text{C-F} \end{cases} \\
&\overline{\sigma}_x = \frac{h}{q_0 L}\sigma_x\left(\frac{L}{2},\frac{h}{2}\right) \\
&\sigma_{xy} = \frac{h}{q_0 L}\sigma_x(0,0)
\end{aligned} \tag{4.1}$$

The nondimensional displacements and stresses of S-S FG beams derived from our proposed model are demonstrated in Tables 4.2 - 4.4. Specifically, we conducted comparative analysis with the quasi-3D model developed by Vo et al. [102], the analytical solution grounded in Reddy's TSDT proposed by Thai and Vo [141], and the third-order shear deformation theory established by Li et al. [168]. Our findings reveal substantial convergence across these different models, confirming the reliability of our model's accuracy in predicting static behavior.

Looking at Tables 4.2-4.4, we observe that the increasing in the power-law index value p, the nondimensional displacement and normal stress are consistently rise because the material graduation change from ceramic to metallic compositions, whereas nondimensional shear stress initially declining until p=5, after which it begins to escalate (see Figure 4.1). The shear stress calculations were performed without implementing a shear correction factor, and notably, the dimensionless shear stress remains constant regardless of the length-to-thickness ratio. Our finding align remarkably well with Reddy's TSDT developed by Thai and Vo [141].

For more demonstration, Figure 4.2 depicts dimensionless displacement variation across different power-law index values for FG beam configurations with length-to-thickness ratio of 5 and 10 under UDL. As the power-law index escalates, the metallic volume fraction correspondingly increases, resulting in progressive reduction of the beam's rigidity. Consequently, this compositional shift is reflected as an increase in the displacement.

Expanding the comparative analysis, Tables 4.5 and 4.6 showcase the dimensionless displacement of Clamped-Clamped (C-C) and Clamped-Free (C-F) functionally graded beams. These results demonstrate good concordance with alternative approaches, including first-order shear deformation theory (FSDT) by Jing et al. [99], and the quasi-3D and third-order shear deformation theory (TSDT) proposed by Vo et al. [102].

Table 4.2 Dimensionless displacements $\overline{w}$ of S-S FG beams

L/h	p	N° elements						Quasi-3D [102]	Reddy [141]	TSDT [168]
		25	50	100	150	200	250			
5	0	3.1160	3.1546	3.1629	3.1644	3.1650	3.1652	3.1397	3.1657	3.1657
	1	6.1471	6.2343	6.2535	6.2570	6.2583	6.2589	6.1338	6.2594	6.2599
	2	7.9548	8.0589	8.0814	8.0856	8.0871	8.0878	7.8606	8.0677	8.0602
	5	9.7645	9.8632	9.8835	9.8872	9.8886	9.8893	9.6037	9.8281	9.7802
	10	10.9016	11.0020	11.0221	11.0258	11.0272	11.0278	10.7572	10.9381	10.8979
20	0	2.3956	2.7541	2.8594	2.8797	2.8869	2.8903	2.8947	2.8962	2.8962
	1	4.6527	5.4699	5.7174	5.7657	5.7828	5.7908	5.7201	5.8049	5.8049
	2	6.0812	7.0529	7.3418	7.3978	7.4177	7.4270	7.2805	7.4421	7.4415
	5	7.5988	8.4856	8.7354	8.7833	8.8002	8.8081	8.6479	8.8182	8.5151
	10	8.4902	9.3688	9.6122	9.6586	9.6750	9.6826	9.5749	9.6905	9.6879

Table 4.3 Dimensionless normal stress $\bar{\sigma}_x$ of S-S FG beam

L/h	P	N° element						Quasi-3D	Reddy	TSDT
		25	50	100	150	200	250	[102]	[141]	[168]
5	0	3,6960	3,7360	3,7460	3,7480	3,7491	3,7494	3.8005	3.8020	3.8020
	1	5,7000	5,7700	5,7900	5,7920	5,7942	5,7948	5.8812	5.8836	5.8837
	2	6,6667	6,7400	6,7600	6,7640	6,7658	6,7665	6.8818	6.8826	6.8812
	5	7,8520	7,9160	7,9360	7,9400	7,9412	7,9418	8.1140	8.1106	8.1030
	10	9,4260	9,4940	9,5160	9,5200	9,5211	9,5217	9.7164	9.7122	9.7063
20	0	12,4269	14,2569	14,8072	14,9137	14,9514	14,9689	15.0125	15.0129	15.0130
	1	18,6113	21,8348	22,8311	23,0255	23,0944	23,1264	23.2046	23.2053	23.2054
	2	22,1520	25,6382	26,6978	26,9036	26,9764	27,0103	27.0988	27.0991	27.0989
	5	27,4094	30,5447	31,4556	31,6301	31,6917	31,7204	31.8137	31.8130	31.8112
	10	33,4069	36,7880	37,7571	37,9420	38,0073	38,0376	38.1600	38.1385	38.1372

Table 4.4 Dimensionless shear stress $\bar{\sigma}_{xz}$ of S-S FG beam

L/h	p	N° element						Quasi-3D	Reddy	TSDT
		25	50	100	150	200	250	[102]	[141]	[168]
5	0	0,7200	0,7350	0,7426	0,7450	0,7463	0,7470	0.7233	0.7332	0.7500
	1	0,7200	0,7350	0,7426	0,7450	0,7463	0,7470	0.7233	0.7332	0.7500
	2	0,6698	0,6836	0,6906	0,6930	0,6941	0,6948	0.6622	0.6706	0.6787
	5	0,5986	0,6112	0,6174	0,6194	0,6205	0,6211	0.5840	0.5905	0.5790
	10	0,6590	0,6728	0,6796	0,6818	0,6830	0,6837	0.6396	0.6467	0.6436
20	0	0,7200	0,7350	0,7425	0,7450	0,7463	0,7470	0.7432	0.7451	0.7500
	1	0,7200	0,7350	0,7425	0,7450	0,7463	0,7470	0.7432	0.7451	0.7500
	2	0,6697	0,6837	0,6907	0,6930	0,6941	0,6948	0.6809	0.6824	0.6787
	5	0,5987	0,6112	0,6174	0,6195	0,6205	0,6212	0.6010	0.6023	0.5790
	10	0,6590	0,6727	0,6796	0,6819	0,6830	0,6837	0.6583	0.6596	0.6436

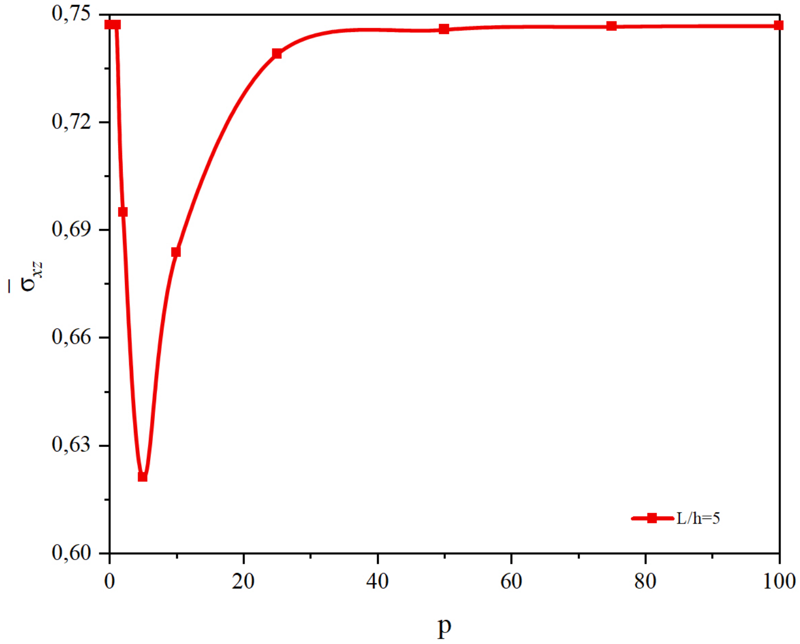

Figure 4.1 Variation of dimensionless shear stress versus power-law index of S-S FG beam

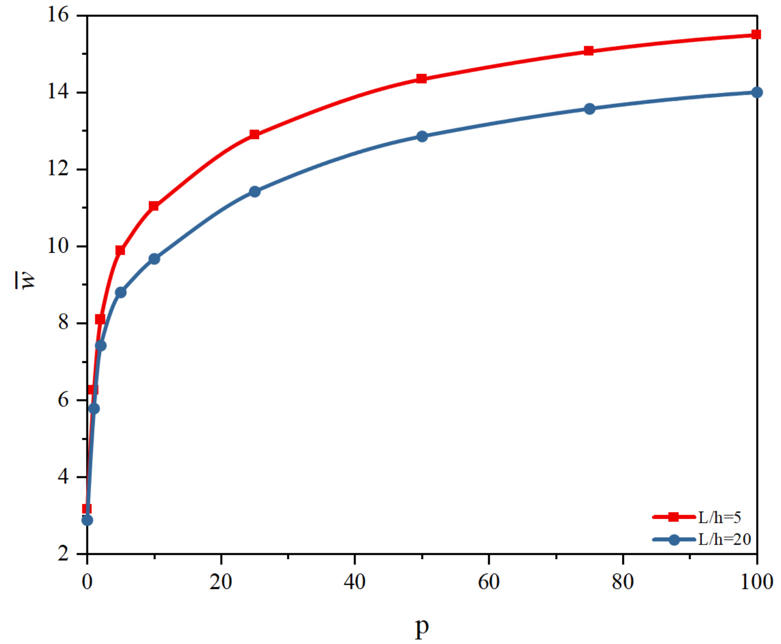

Figure 4.2 Variation of dimensionless Displacement versus power-law index of S-S FG beam

Table 4.5 Dimensionless displacements $\overline{w}$ of C-C FG beams

L/h	p	N° elements						FBT	Quasi-3D	TSDT
		25	**50**	**100**	**150**	**200**	**250**	**[99]**	**[102]**	**[102]**
5	**0**	0,8498	0,8603	0,8623	0,8627	0,8629	0,8629	0.8590	0.8328	0.8501
	1	1,6112	1,6340	1,6387	1,6396	1,6399	1,6400	1.6339	1.5722	1.6179
	2	2,1335	2,1613	2,1668	2,1679	2,1682	2,1684	2.1523	2.0489	2.1151
	5	2,8542	2,8826	2,8879	2,8888	2,8892	2,8894	2.8420	2.6929	2.7700
	10	3,3061	3,3359	3,3413	3,3423	3,3426	3,3428	3.2516	3.1058	3.1812
20	**0**	0,4910	0,5647	0,5861	0,5903	0,5917	0,5924	0.5896	0.5894	0.5933
	1	0,9500	1,1172	1,1675	1,1773	1,1808	1,1824	1.1774	1.1613	1.1843
	2	1,2444	1,4437	1,5024	1,5138	1,5179	1,5198	1.5124	1.4811	1.5203
	5	1,5689	1,7525	1,8036	1,8134	1,8169	1,8185	1.8070	1.7731	1.8155
	10	1,7604	1,9431	1,9931	2,0026	2,0060	2,0075	1.9921	1.9694	2.027

Table 4.6 Dimensionless displacements $\overline{w}$ of C-F FG beams

L/h	p	N° elements						FBT	Quasi-3D	TSDT
		25	**50**	**100**	**150**	**200**	**250**	**[99]**	**[102]**	**[102]**
5	**0**	28,4313	28,6928	28,7589	28,7711	28,7755	28,7777	28.7805	28.5524	28.7555
	1	56,5458	57,1671	57,3247	57,3537	57,3642	57,3694	57.3822	56.2002	57.3323
	2	72,8335	73,5540	73,7364	73,7701	73,7822	73,7883	73.7757	71.7295	73.6482
	5	87,7477	88,3595	88,5138	88,5422	88,5525	88,5579	88.4251	86.1201	88.2044
	10	97,1248	97,7168	97,8659	97,8933	97,9033	97,9086	97.6052	95.7582	97.4151
20	**0**	23,0002	26,3555	27,3537	27,5468	27,6151	27,6471	27.7125	27.6217	27.7029
	1	44,6957	52,3742	54,7258	55,1845	55,3471	55,4231	55.5384	54.6285	55.5546
	2	58,4002	67,5101	70,2511	70,7831	70,9716	71,0596	71.1923	69.5266	71.2051
	5	72,8754	81,1142	83,4746	83,9267	84,0864	84,1611	84.2889	82.4836	84.2712
	10	81,3719	89,5002	91,7937	92,2311	92,3856	92,4579	92.5726	91.2606	92.5571

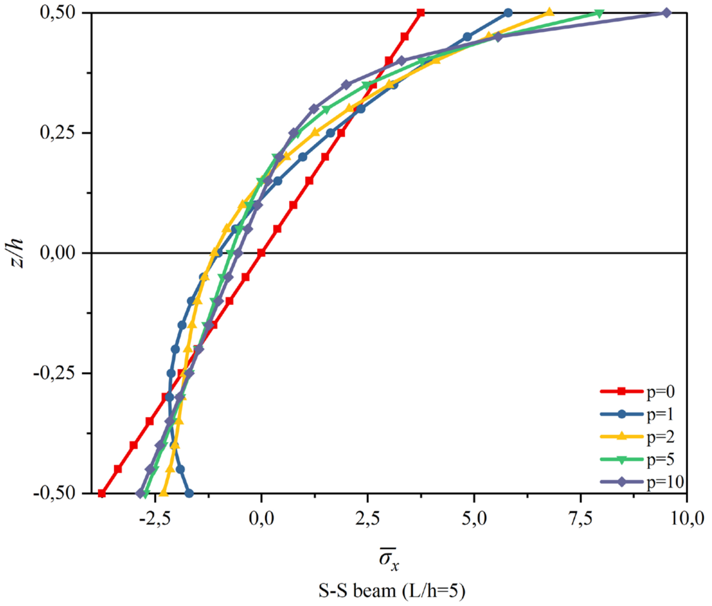

Figure 4.3 Dimensionless normal stress distribution through the thickness of S-S FG beam for various power-law index values

The distribution of stresses across the depth of S-S FG beam has been analyzed in Figure 4.3 and 4.4.

Figure 4.3 illustrate the normalized stress distribution across the beam's thickness for various power-law index values. The analysis reveals that as the power-law index increases, the nondimensional normal stress also rises. The stress pattern demonstrates tensile at the beam's upper surface and compressive at its lower surface. Notably, when the beam is homogeneous, the compressive stress reaches its maximum at the bottom, while tensile stress is minimal at the top.

Figure 4.4 highlights the dimensionless shear stress distribution over the thickness with multiple power-law index values. It can be observed that the shear stress is perfectly quadratic and symmetric over the thickness for p=0 and asymmetrical for the other values of p, and the shear stress is zero at the top and bottom surfaces of the beam.

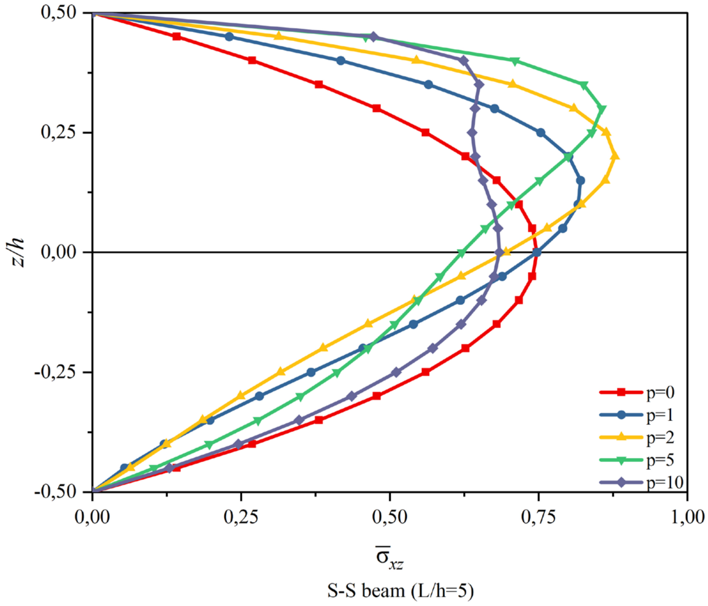

Figure 4.4 Dimensionless shear stress distribution through the thickness of S-S FG beam for various power-law index values p

4.4. Buckling analysis of FG beams

In the next examples the present element is used for mechanical and thermal buckling analysis of FG beams.

4.4.1. Mechanical buckling

The analysis was conducted to evaluate the mechanical buckling response of Al_2O_3/Al FG beams subjected to axial compressive load based on the proposed model. The research analyzes how power-law index, length-to-depth ratio, and boundary conditions affect the critical buckling load. A nondimensional representation of the critical buckling load is derived using the following equation:

$$\overline{P}_{cr} = P_{cr} \frac{12L^2}{h^3 E_m} \tag{4.2}$$

Tables 4.7 - 4.9 present the convergence of dimensionless critical buckling loads across different power-law index values, length-to-depth ratio, and ends support. The findings were validated against several established approaches, including Timoshenko beam theory (TBT) implemented by Li and Batra [109], the hyperbolic shear deformation beam theory (HSDBT) developed by Nguyen et al. [126], and First-order shear deformation theory (FSDT) utilized by Kahya and Turan [116]. The comparative analysis reveals strong consistency between the present model and previous theories, with particular concordance to HSDBT of Nguyen et al. [126].

Results in Tables 4.7-4.9 reveal that higher values of p correspond to lower nondimensional critical buckling loads, with increased length-to-thickness ratio results in elevated critical buckling loads.

Table 4.7 Dimensionless critical buckling loads $\overline{P}_{cr}$ of S-S Al_2O_3/Al FG beam

L/h	P	N° elements						TBT	HSDBT	FSDT
		25	**50**	**100**	**150**	**200**	**250**	**[109]**	**[126]**	**[116]**
	0	49,2643	48,7500	48,6429	48,6000	48,6000	48,6000	48.835	48.8406	48.5907
	1	24,9857	24,6857	24,6000	24,6000	24,5786	24,5786	24.687	24.6894	24.5815
5	**2**	19,3071	19,0929	19,0286	19,0286	19,0286	19,0286	19.245	19.1577	19.1617
	5	15,7131	15,5848	15,5528	15,5469	15,5448	15,5437	16.024	15.7355	15.9417
	10	14,0688	13,9664	13,9407	13,9360	13,9344	13,9335	14.427	14.1448	14.3445
	0	55,0286	52,9714	52,4571	52,2857	52,2857	52,2857	52.309	52.3083	-
	1	27,7689	26,5474	26,2423	26,1859	26,1662	26,1569	26.171	26.1707	-
10	**2**	21,4994	20,6385	20,4235	20,3837	20,3698	20,3633	20.416	20.3909	-
	5	17,7451	17,2251	17,0954	17,0712	17,0628	17,0589	17.192	17.1091	-
	10	16,0190	15,6024	15,4983	15,4791	15,4723	15,4690	15.612	15.5278	-

Table 4.8 Dimensionless critical buckling loads $\overline{P}_{cr}$ of C-C Al_2O_3/Al FG beam

L/h	p	N° elements						TBT	HSDBT	FSDT
		25	**50**	**100**	**150**	**200**	**250**	**[109]**	**[126]**	**[116]**
	0	154,4571	152,5714	152,0786	151,9929	151,9714	151,9500	154.35	154.5610	151.9430
	1	80,9143	79,7571	79,4786	79,4357	79,4143	79,3929	80.498	80.5940	79.3903
5	**2**	61,3500	60,5571	60,3429	60,3214	60,3000	60,3000	62.614	61.7666	61.7449
	5	46,5181	46,0601	45,9459	45,9248	45,9174	45,9138	50.384	47.7174	49.5828
	10	40,3938	40,0357	39,9465	39,9300	39,9241	39,9214	44.267	41.7885	43.5014
	0	205,3714	197,1429	195,0857	194,7429	194,5714	194,4000	195.34	195.3623	-
	1	104,8217	99,9439	98,7298	98,5053	98,4266	98,3899	98.749	98.7885	-
10	**2**	80,6484	77,2155	76,3610	76,2031	76,1477	76,1218	76.980	76.6538	-
	5	64,9131	62,8522	62,3391	62,2443	62,2111	62,1955	64.096	62.9580	-
	10	57,9209	56,2752	55,8653	55,7895	55,7630	55,7505	57.708	56.5926	-

The relationship between power-law index and critical buckling loads has been examined using FG beams with length-to-thickness ratio of 5 and 10, as illustrated in Figure 4.5. The results show a marked decrease in dimensionless critical buckling load with increasing p values, corresponding to the shift from rigid ceramic-rich composition to more flexible metal-rich beam.

Table 4.9 Dimensionless critical buckling loads $\overline{P}_{cr}$ of C-F Al_2O_3/Al FG beam

L/h	p	N° elements						TBT [109]	HSDBT [126]	FSDT [116]
		25	50	100	150	200	250			
5	0	13,2214	13,0929	13,0714	13,0714	13,0714	13,0714	13.213	13.0771	13.0594
	1	6,6429	6,5571	6,5357	6,5357	6,5357	6,5357	6.6002	6.5427	6.5352
	2	5,1643	5,1000	5,1000	5,1000	5,0786	5,0786	5.1495	5.0977	5.0981
	5	4,3063	4,2738	4,2657	4,2642	4,2637	4,2634	4.3445	4.2772	4.2926
	10	3,9006	3,8746	3,8681	3,8669	3,8664	3,8662	3.9502	3.8820	3.8970
10	0	14,0571	13,5429	13,3714	13,3714	13,3714	13,3714	13.349	13.3741	-
	1	7,0473	6,7421	6,6658	6,6518	6,6468	6,6446	6.6571	6.6678	-
	2	5,4655	5,2503	5,1967	5,1867	5,1831	5,1816	5.1945	5.2025	-
	5	4,5423	4,4124	4,3800	4,3740	4,3718	4,3709	4.3902	4.3974	-
	10	4,1139	4,0099	3,9838	3,9790	3,9773	3,9765	3.9969	4.0045	-

An investigation of length-to-thickness ratio effects on mechanical buckling response has been conducted for FG beams with various ends conditions at p=5, as shown in Figure 4.6. The figure shows that nondimensional critical buckling loads increase with higher L/h values for all boundary conditions. Therefore, slender FG beams have the lower buckling resistance. Maximum critical loads are observed in double-clamped support, characterized by rapid initial increase at small L/h ratios followed by stabilization at higher values of L/h. While Clamped-free condition exhibit the lowest critical loads, largely unaffected by higher length-to-thickness variations.

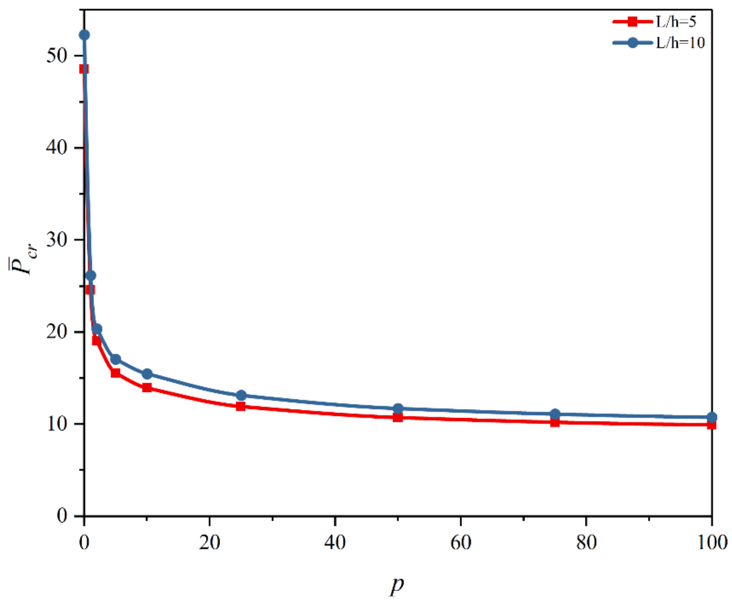

Figure 4.5 The influence of power-law index p on nondimensional Critical buckling load of S-S FG beam

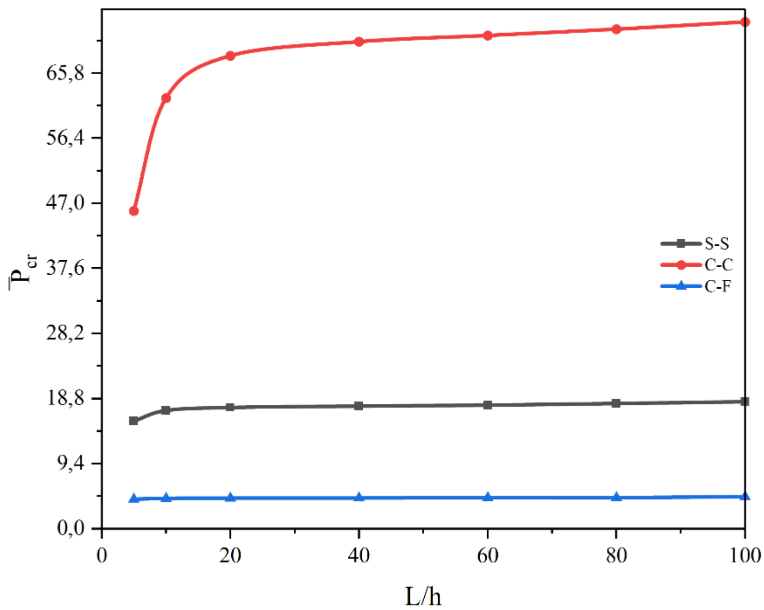

Figure 4.6 Variation of nondimensional critical buckling load of FG beam (L/h=5) with various ends conditions under compressive axial load

4.4.2. Thermal buckling FG beams

This section examines thermal buckling response of Si_3N_4/SUS304 functionally graded beams with double clamped (C-C) boundary conditions under uniform temperature rise. The material properties utilized in this analysis, presented in Table 4.1, are considered temperature-independent.

In reviewing existing literatures, we discovered that thermal buckling analysis with temperature-independent properties has been addressed in single publication [123]. This work, which employs multiple beam theories, was selected as our comparative reference.

First, a convergence study was conducted in Table 4.10. This study aims to validate the developed model for critical temperature loads of FG beams. The results show that as the number of elements increases, the critical temperature decreases and approaches stable, converged values. At 250 elements, the change compared to 200 elements is small, indicating the reliability and stability of the numerical model. Furthermore, the close agreement between the results obtained and the reference values from Timoshenko beam theory (TBT) demonstrates the accuracy of the present model.

To underscore the proposed element's precision, Table 4.11 presents comprehensive comparative study of critical temperature predictions. The results show remarkable consistency with Reddy's theory and Exponential shear deformation theory (ESDT) [123], evaluated across multiple p values and length-to-thickness ratios.

Table 4.10 Convergence study of critical temperature ΔT_{cr} of Si_3N_4/SUS304 FG beam (L/h=25) with Clamped ends

p	N° elements					TBT [123]
	50	100	150	200	250	
0.5	553.1370	520.8516	514.8805	512.7899	511.8172	510.002
1	496.7870	468.2881	463.0174	461.1719	460.3143	458.780
2	456.8361	431.8179	427.1909	425.5709	424.8185	423.624
5	423.6043	401.5573	397.4799	396.0522	395.3897	394.488
10	404.1771	383.0424	379.1336	377.7650	377.1302	376.223

Figure 4.7 illustrates the impact of length-to-thickness ratio on critical temperature for C-C Si3N4/SUS304 FG beam under uniform temperature rise for various material gradations. The results demonstrate a significant decrease in critical temperature as L/h increases across all power-index values. Pure ceramic beams (p=0) exhibit the highest critical temperatures, which can be attributed to the superior thermal resistance and stiffness of Si3N4. Additionally, the Figure indicates diminished temperature sensitivity at higher L/h values.

Table 4.11 Comparison of critical Temperature ΔT_{cr} of C-C Si_3N_4/SUS304 FG beam

L/h	Model	p=0	p=1	p=2	p=5	p=10
	Present	1075.085	712.028	656.860	611.0733	582.879
20	**Reddy [123]**	-	710.491	655.616	610.086	581.957
	ESDT [123]	-	710.597	655.696	610.150	582.054
	Present	485.791	321.684	296.931	276.421	263.650
30	**Reddy [123]**	-	320.154	295.608	275.276	262.557
	ESDT [123]	-	320.176	295.624	275.289	262.577
	Present	275.593	182.490	168.461	156.841	149.593
40	**Reddy [123]**	-	180.966	167.128	155.672	148.474
	ESDT [123]	-	180.972	167.133	155.676	148.480

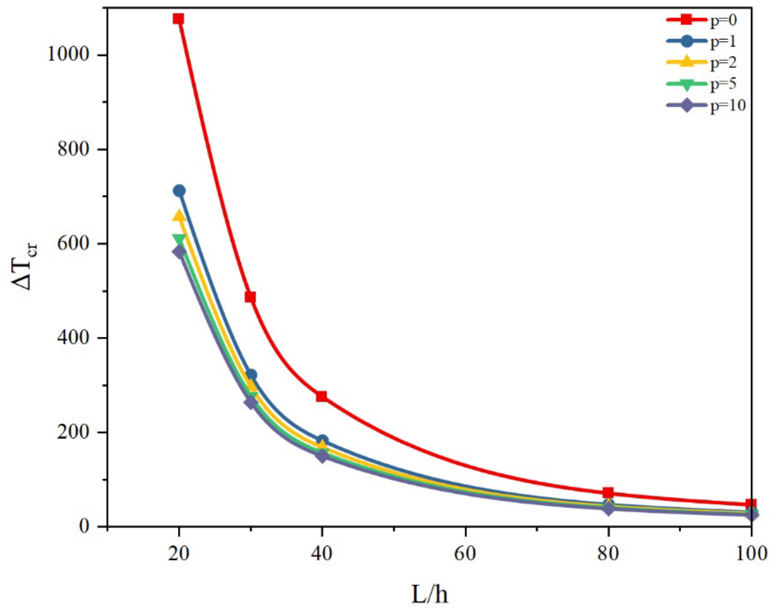

Figure 4.7 The effect of length-to-thickness ratio on the critical temperature ΔT_{cr} of C-C Si_3N_4/SUS304 beam

4.5. Free vibration of FG beams

This section presents a numerical analysis of the free vibration behavior of FG beams with three different support ends. The model performance is validated through convergence studies and comparison against established results from the literature.

The beam is combined of alumina (Al_2O_3) and aluminum (Al), which their material properties are listed in Table 4.1.

For convenience, following nondimensional natural frequency parameter is used in presenting the numerical results.

$$\varpi = \frac{\omega L^2}{h}\sqrt{\frac{\rho_m}{E_m}} \tag{4.3}$$

Just like the mentioned in above analysis, as shown in Tables 4.12 – 4.14 , the proposed model gives fast converged results of dimensionless natural frequencies ϖ to the references solutions for all boundary condition and length-to thickness ratio. Furthermore, the obtained results are in good agreement with literatures values from Unified and Integrated Timoshenko beam theory (UI) developed by Katili et al. [150], First-order beam theory (FBT) of Vo et al. [97], and Levinson beam theory (LBT) of Wang and Li [145], demonstrate the accuracy of the ETBT. The results of C-C FG beam exhibit the highest natural frequencies compared to S-S and C-F. As predicted the beam Young's modulus and rigidity decrease as the power law index increases leading to lower natural frequencies. All three boundary conditions share the same pattern.

Table 4.12 Comparison of the dimensionless natural frequencies ϖ of S-S Al_2O_3/Al FG beam

L/h	**p**	**N° elements**					**UI**	**FBT**	**LBT**
		50	**100**	**150**	**200**	**250**	**[150]**	**[97]**	**[145]**
5	**0**	5.1624	5.1549	5.1536	5.1531	5.1529	5.1526	5.1526	5.1525
	1	3.9992	3.9926	3.9913	3.9909	3.9907	3.9790	3.9710	3.9902
	2	3.6293	3.6237	3.6227	3.6224	3.6222	3.6228	3.6049	3.6280
	5	3.3961	3.3922	3.3914	3.3912	3.3911	3.4178	3.4025	3.4090
	10	3.2729	3.2695	3.2689	3.2687	3.2686	3.3022	3.2962	3.2873
20	**0**	5.6004	5.4957	5.4761	5.4692	5.4660	5.4603	5.4603	5.4603
	1	4.3327	4.2373	4.2194	4.2131	4.2102	4.2049	4.2038	4.2050
	2	3.9413	3.8625	3.8477	3.8425	3.8401	3.8369	3.8349	3.8363
	5	3.7200	3.6659	3.6558	3.6523	3.6506	3.6506	3.6490	3.6491
	10	3.5999	3.5536	3.5450	3.5419	3.5405	3.5411	3.5404	3.5395

Table 4.13 Comparison of the dimensionless natural frequencies of C-F Al_2O_3/Al FG beam

L/h	p	N° elements					UI [150]	FBT [97]	LBT [145]
		50	100	150	200	250			
5	0	1.8974	1.8952	1.8947	1.8946	1.8945	1.8944	1.8944	1.9387
	1	1.4655	1.4635	1.4631	1.4629	1.4629	1.4637	1.4627	1.4917
	2	1.3334	1.3317	1.3314	1.3313	1.3313	1.3358	1.3335	1.3623
	5	1.2580	1.2568	1.2566	1.2565	1.2565	1.2661	1.2642	1.2989
	10	1.2163	1.2153	1.2151	1.2151	1.2150	1.2244	1.2237	1.2623
20	0	1.9989	1.9620	1.9551	1.9527	1.9515	1.9495	1.9495	1.9526
	1	1.5460	1.5124	1.5061	1.5039	1.5028	1.5012	1.5010	1.5030
	2	1.4067	1.3789	1.3737	1.3719	1.3710	1.3700	1.3697	1.3716
	5	1.3285	1.3096	1.3060	1.3048	1.3042	1.3040	1.3037	1.3062
	10	1.2860	1.2698	1.2668	1.2657	1.2652	1.2650	1.2649	1.2676

Table 4.14 Comparison of the dimensionless natural frequencies of C-C Al_2O_3/Al FG beam

L/h	p	N° elements					UI [150]	FBT [97]
		50	100	150	200	250		
5	0	10.0168	10.0023	9.9997	9.9987	9.9982	9.9982	9.9983
	1	7.9176	7.9043	7.9019	7.9010	7.9006	7.9364	7.9015
	2	7.1064	7.0954	7.0934	7.0927	7.0924	7.2632	7.1901
	5	6.3714	6.3640	6.3627	6.3622	6.3620	6.6998	6.6446
	10	6.0253	6.0191	6.0191	6.0175	6.0173	6.3365	6.3160
20	0	12.5346	12.2995	12.2555	12.2400	12.2328	12.2201	12.2202
	1	9.7161	9.5017	9.4615	9.4474	9.4408	9.4417	9.4311
	2	8.8283	8.6514	8.6182	8.6066	8.6011	8.6247	8.6046
	5	8.2945	8.1735	8.1509	8.1430	8.1393	8.1863	8.1697
	10	8.0095	7.9061	7.8868	7.8800	7.8768	7.9186	7.9115

4.5.1. Free vibration in thermal environment

A thorough review of existing literature concerning free vibration behavior of FG beams in thermal environments, specifically those with temperature independent material properties, identified a notable research gap in heated FG beam analysis. This study fills this void by analyzing the effect of uniform temperature rise on natural frequencies of Clamped-Clamped FG beam.

The dimensionless natural frequencies of C-C FG beam made of Al_2O_3/Al under uniform temperature rise ΔT with L/h=20 and various power law index values are presented in Figure 4.8. As the temperature increases, the natural frequencies consistently decrease, indicating a reduction in beam stiffness due heating, regardless of the power law index value. When p=0, the beam exhibit the highest natural frequencies across all temperatures. As the power law index increases, the natural frequencies progressively decreases, with p=5 showing the lowest values.

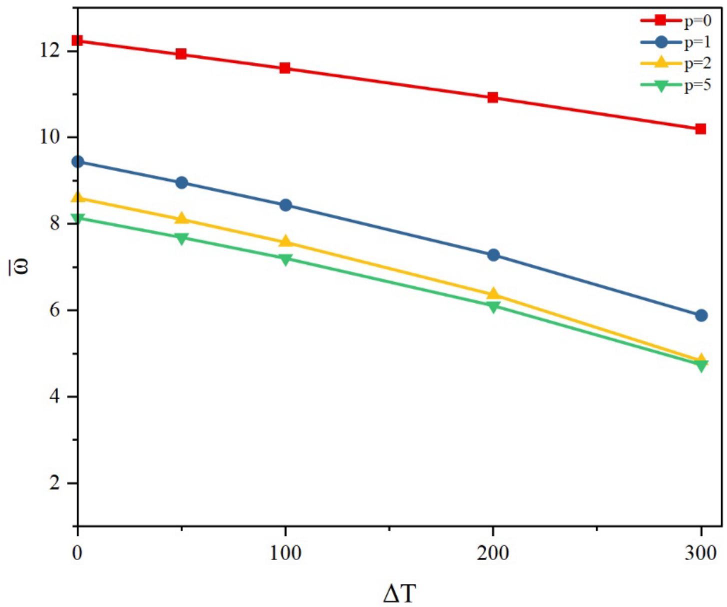

Figure 4.8 Dimensionless natural frequencies of C-C FG beam with L/h=20 under uniform temperature rise

4.6. Conclusion

This chapter has demonstrated the effectiveness of the Enhanced Timoshenko beam theory (ETBT) through extensive numerical analysis. The investigation, covering static, mechanical and thermal buckling, and free vibration of functionally graded beams, yielded results that align closely with established literature. Specifically, the calculation of displacements, stresses, critical loads and temperatures, and natural frequencies. Additionally, parametric studies reveal valuable insight into how beam behavior is influenced by length-to-thickness ratio, boundary conditions, and power-law index.

Chapter 5:
Application ETBT on FG sandwich beams-Results and discussions

5.1. Introduction

This chapter presents various numerical examples demonstrating, performance of the developed element in analyzing FG sandwich beams' buckling, and free vibration behaviors. Obtained results, encompassing nondimensional natural frequencies and critical loads, are validated against established literature findings. The analysis explore the impact of various parameters including support conditions, length-to-depth ratio.

5.2. FG sandwich beams analysis

Based on the mathematical formulation of enhanced Timoshenko beam theory (ETBT) presented in chapter 3, a computational code is developed to analyze mechanical buckling and free vibration of FG sandwich beam.

5.3. Mechanical buckling of FG sandwich Beams

Mechanical buckling analysis is conducted for sandwich beam featuring two support conditions: simply supported (S-S) and cantilever (C-F). These beams incorporate FG skins surrounding an isotropic ceramic core. The element accuracy is validated through comparison with established results. The beam utilizes a combination of alumina and aluminum materials, whose properties are specified in Table 4.1

The analysis explores the effect of power-law index and length-to-thickness ratio on the critical loads. Three distinctive sandwich beam layouts were analyzed (1-1-1, 2-1-2, 2-2-1). The numerical model implemented 250 elements, reflecting optimal convergence, which is determined in the previous analysis. The numerical findings are presented in Tables 5.1-5.4

Tables 5.1-5.4 presents the comparison study of FG sandwich beams' dimensionless critical buckling loads, examining the variation in boundary conditions, length-to-thickness ratio, and power-law index values. The ETBT's results show remarkable consistency with the literature, including the analytical solution based on HSDT developed by Nguyen et al. [126] and Nguyen and Nguyen [128], as well as FE solution utilizing refined shear deformation theory (RSDT) by Vo et al. [130]. Notable findings indicate that the critical buckling loads are significantly influenced by both material graduation and the sandwich beam layouts, with the (2-2-1) configuration displays highest critical loads, while the (2-1-2) layout exhibits the lowest critical buckling loads across all tested conditions.

Table 5.1 Comparison of dimensionless critical buckling loads of S-S FG sandwich beams with ceramic core (L/h=5)

L/h	p	Model	1-1-1	2-1-2	2-2-1
5	1	**Present**	24.5705	22.2150	26.0410
		HSDT [126]	24.5602	22.2121	26.3611
		RSDT [130]	24.5596	22.2108	26.3611
		HSDT [128]	24.5598	22.2113	26.3609
	2	**Present**	18.3848	15.9259	20.2664
		HSDT [126]	18.3596	15.9167	20.3751
		RSDT [130]	18.3587	15.9152	20.3750
		HSDT [128]	18.3591	15.9158	20.3748
	5	**Present**	13.7330	11.6607	15.7230
		HSDT [126]	13.7226	11.6697	15.7313
		RSDT [130]	13.7212	11.6676	15.7307
		HSDT [128]	13.7218	11.6685	15.7307
	10	**Present**	12.2626	10.5178	14.2131
		HSDT [126]	12.2621	10.5370	14.2002
		RSDT [130]	12.2605	10.5348	14.1995
		HSDT [128]	12.2611	10.5356	14.1995

Table 5.2 Comparison of dimensionless critical buckling loads of S-S FG sandwich beams with ceramic core (L/h=20)

L/h	p	Model	1-1-1	2-1-2	2-2-1
20	1	**Present**	26.0974	23.5057	27.6699
		HSDT [126]	25.9588	23.4212	27.9537
		RSDT [130]	25.9588	23.4211	27.9540
		HSDT [128]	25.9588	23.4212	27.9537
	2	**Present**	19.3161	16.6815	21.3153
		HSDT [126]	19.2000	16.6051	21.3923
		RSDT [130]	19.3116	16.6050	21.3927
		HSDT [128]	19.1999	16.6050	21.3923
	5	**Present**	14.3250	12.1520	16.4165
		HSDT [126]	14.2285	12.0886	16.3829
		RSDT [130]	14.2284	12.0883	16.3834
		HSDT [128]	14.2285	12.0885	16.3829
	10	**Present**	12.7707	10.9637	14.8120
		HSDT [126]	12.6820	10.9075	14.7520
		RSDT [130]	12.6819	10.9075	14.7525
		HSDT [128]	12.6819	10.9074	14.7520

Table 5.3 Comparison of dimensionless critical buckling loads of cantilever FG sandwich beams with ceramic core (L/h=5)

L/h	p	Model	1-1-1	2-1-2	2-2-1
5	1	**Present**	6.4184	5.7934	6.8153
		HSDT [126]	6.4166	5.7922	6.9050
		RSDT [130]	6.4166	5.7921	6.9050
	2	**Present**	4.7591	4.1172	5.2582
		HSDT [126]	4.7564	4.1157	5.2952
		RSDT [130]	4.7564	4.1156	5.2952
	5	**Present**	3.5327	3.0007	4.0532
		HSDT [126]	3.5311	3.0006	4.0621
		RSDT [130]	3.5310	3.0004	4.0620
	10	**Present**	3.1498	2.7073	3.6575
		HSDT [126]	3.1489	2.7078	3.6596
		RSDT [130]	3.1488	2.7077	3.6595

Table 5.4 Comparison of dimensionless critical buckling loads of cantilever FG sandwich beams with ceramic core (L/h=20)

L/h	p	Model	1-1-1	2-1-2	2-2-1
20	1	**Present**	6.5388	5.8924	6.9378
		HSDT [126]	6.5083	5.8713	7.0096
		RSDT [130]	6.5083	5.8713	7.0096
	2	**Present**	4.8380	4.1794	5.3416
		HSDT [126]	4.8110	4.1603	5.3615
		RSDT [130]	4.8110	4.1603	5.3615
	5	**Present**	3.5870	3.0436	4.1123
		HSDT [126]	3.5637	3.0276	4.1042
		RSDT [130]	3.5637	3.0275	4.1043
	10	**Present**	3.1975	2.7461	3.7098
		HSDT [126]	3.1759	2.7317	3.6952
		RSDT [130]	3.1759	2.7317	3.6952

5.4. Free vibration of FG sandwich beams

The study proceeds with an investigation of the natural frequencies ω in sandwich beams constructed with FG surface layers and a homogenous ceramic core. The beam composition consists of Al_2O_3 and Al.

Tables 5.5-5.8 document the evaluation of dimensionless natural frequencies across different sandwich beam configurations, incorporating various length-to-depth ratios, power-law indices, and structural layouts (1-1-1, 2-1-2, 2-2-1). The analysis of simply supported (S-S) sandwich beams, detailed in Tables 5.5 and 5.6, includes comparisons with Refined sheard deformation theory (RSDT) [130] and high-order zigzag theory (HOZT) [169]. Similarly, Tables 5.7 and 5.8 analyze C-C configuration, with results validate against RSDT [130] and quasi-3D [170]. For all cases, the 2-2-1 layout exhibit the highest natural frequencies due to stiffer ceramic core, while 2-1-2 layout exhibit the lowest natural frequencies because its softer FG distribution. For each layout, natural frequencies decrease as the value of p increases , reflecting the reduce of stiffness associated with higher metallic content in FG layer. In general, The proposed model align closely with published works, particularly with HOZT and quasi-3D. Overall, the developed ETBT is efficient in predicting free vibration behavior.

Table 5.5 Comparison of dimensionless natural frequencies S-S FG sandwich beams with ceramic core (L/h=5)

L/h	p	Model	1-1-1	2-1-2	2-2-1
5	1	**Present**	3.9815	3.7852	4.1071
		RSDT [130]	3.8756	3.7298	3.9911
		HOZT [169]	3.8421	3.7164	3.9830
	2	**Present**	3.5526	3.3061	3.7161
		RSDT [130]	3.4190	3.2366	3.5719
		HOZT [169]	-	-	-
	5	**Present**	3.1754	2.9262	3.3749
		RSDT [130]	3.0182	2.8441	3.1966
		HOZT [169]	3.0399	2.8974	3.2808
	10	**Present**	3.0507	2.8260	3.2656
		RSDT [130]	2.8810	2.7357	3.0630
		HOZT [169]	2.9203	2.8005	3.1639

Table 5.6 Comparison of dimensionless natural frequencies S-S FG sandwich beams with ceramic core (L/h=20)

L/h	p	Model	1-1-1	2-1-2	2-2-1
20	1	**Present**	4.1691	3.9561	4.2029
		RSDT [130]	4.0328	3.8768	4.1602
		HOZT [169]	3.9977	3.8661	4.1536
	2	**Present**	3.7067	3.4427	3.7852
		RSDT [130]	3.5389	3.3465	3.7049
		HOZT [169]			
	5	**Present**	3.3064	3.0423	3.4226
		RSDT [130]	3.1111	2.9310	3.3028
		HOZT [169]	3.1451	3.0081	3.4043
	10	**Present**	3.1746	2.9382	3.3051
		RSDT [130]	2.9662	2.8188	3.1613
		HOZT [169]	3.0262	2.9199	3.2865

Table 5.7 Comparison of dimensionless natural frequencies C-C FG sandwich beams with ceramic core (L/h=5)

L/h	p	Model	1-1-1	2-1-2	2-2-1
5	1	**Present**	8.2230	7.8411	8.4108
		RSDT [130]	7.9580	7.6865	8.1554
		Quai-3D [170]	8.0595	7.7854	8.2615
	2	**Present**	7.4636	6.9625	7.7851
		RSDT [130]	7.1373	6.7826	7.4105
		Quai-3D [170]	7.2328	6.8740	7.5143
	5	**Present**	6.7527	6.2173	7.1863
		RSDT [130]	6.3889	6.0293	6.7188
		Quai-3D [170]	6.4780	6.1124	6.8210
	10	**Present**	6.5061	6.0018	6.9733
		RSDT [130]	6.1240	5.8059	6.4641
		Quai-3D [170]	6.2099	5.8848	6.5654

Table 5.8 Comparison of dimensionless natural frequencies C-C FG sandwich beams with ceramic core (L/h=20)

L/h	p	Model	1-1-1	2-1-2	2-2-1
20	1	**Present**	9.3835	8.9064	9.4583
		RSDT [130]	9.0722	8.7241	9.355
		Quai-3D [170]	9.1061	8.7569	9.3964
	2	**Present**	8.3549	7.7613	8.5299
		RSDT [130]	7.9727	7.5417	8.3430
		Quai-3D [170]	8.0035	7.5711	8.3877
	5	**Present**	7.4598	6.8635	7.7203
		RSDT [130]	7.0170	6.6116	7.4461
		Quai-3D [170]	7.0451	6.6379	7.4955
	10	**Present**	7.1642	6.6285	7.4570
		RSDT [130]	6.6924	6.3590	7.1296
		Quai-3D [170]	6.7194	6.3841	7.1809

5.5. Conclusion

This chapter presents a comprehensive investigation into buckling and free vibration behaviors of three distinct sandwich FGM beams configuration, employing Enhanced Timoshenko beam theory. The findings reveal that FG sandwich beam is influenced by power-law index, length-to-thickness ratio, thickness schematic variation, and boundary condition. Validation through extensive comparison with established literature confirms the model's efficacy in analyzing the buckling and free vibration behaviors of sandwich FGM beam structures.

General Conclusion

The development of functionally graded materials represents a major advance in material science. Featuring unique variation in composition and microstructure properties across the thickness. This class of composites continues to gain prominence in scientific research and engineering applications. The complexity of the design and optimization of these materials demands dedicated research efforts, especially in view of their potential advantages in various fields. The development of tailored methodologies is essential to address the distinctive geometric and material properties intrinsic to FGM.

The present research aims to analyze the static, buckling, and vibrations of functionally graded and sandwich beams, by developing enhanced Timoshenko beam theory (ETBT). Based on ETBT, a two nodded beam element with three degrees of freedom per node had been developed, considering quadratic variation of shear stress along the thickness without introducing any shear correction factor. The accuracy and the performance of the formulated element is confirmed by comparing the obtained results with those from literatures. The effect of the power law index, length-to-thickness ratio, and boundary conditions on static, buckling, and free vibration is investigated. This work has been divided into two parts.

The first part provides an overview of functionally graded materials, encompassing their definition, manufacturing technics, and diverse applications. Subsequent reviews prevalent beam theories employed for analyzing and modeling FG and sandwich beams. A detailed literature review examining static, buckling, and free vibration response of FGM beams is presented.

In the second part, an enhanced Timoshenko beam theory ETBT with three variables has been developed for the analysis of FG and sandwich beams behaviors. The model features quadratic shear stress distribution through the thickness and meets the stress-free conditions on the upper and lower surfaces of the beam without shear correction factor. The physical neutral axis concept mitigates stretching-bending effect. Based ETBT, a beam element was formulated to investigate the static, buckling, and free vibration behaviors of FGM beams. The validation of the developed element was achieved through comparative analysis of displacements, critical temperature and buckling loads, and natural frequencies results against established literatures. The comparison consistently showed excellent agreement, validating the element's effectiveness. Moreover, the influence of different parameters including length-to-thickness, power-law index, and boundery conditions, on the FGM beams behaviors has been explored.

Based on the analysis, the following key findings emerge:

- Based on the findings, the present model ETBT is reliable in predicting the static, buckling, and dynamic behaviors of FGM beam.
- The nondimensional displacement of FG beams decreases by the increasing of length-to-thickness ratio, whereas with it increases as the power law index value increase.
- The dimensionless shear stress of FG beams doesn't effect by the change of length-to-thickness ratio but it decreases with increase of the power-law index until p=5 and then increases again.
- The dimensionless natural frequency and critical buckling load of FG and sandwich beams increase with the increase of the length-to-thickness ratio and decrease with increase of the power law index.
- The critical temperature of FG beams decreases with increase of both length to thickness ratio and power-la index.
- The natural frequencies of FG beams decrease with increase of the temperature.
- The sandwich layout configuration effects on the beam response.

Perspectives

In perspective, it is planned to apply the ETBT for the analysis of thermal behaviors response of FG sandwich beams and to analyze the static, buckling and free vibration response of FG beams using analytical solution.

References

[1] Naebe M, Shirvanimoghaddam K. Functionally graded materials: A review of fabrication and properties. Applied Materials Today. 2016;5:223-45.

[2] Miyamoto Y, Kaysser WA, Rabin BH, Kawasaki A, Ford RG. Introduction. In: Miyamoto Y, Kaysser WA, Rabin BH, Kawasaki A, Ford RG, editors. Functionally Graded Materials: Design, Processing and Applications. Boston, MA: Springer US; 1999. p. 1-6.

[3] Kieback B, Neubrand A, Riedel H. Processing techniques for functionally graded materials. Materials Science and Engineering: A. 2003;362:81-106.

[4] Chen L, Goto T. Chapter 16 - 16.1 Functionally Graded Materials. In: Sōmiya S, Aldinger F, Claussen N, Spriggs RM, Uchino K, Koumoto K, et al., editors. Handbook of Advanced Ceramics. Oxford: Academic Press; 2003. p. 445-64.

[5] Markworth AJ, Ramesh KS, Parks WP. Modelling studies applied to functionally graded materials. Journal of Materials Science. 1995;30:2183-93.

[6] Saleh B, Jiang J, Fathi R, Al-hababi T, Xu Q, Wang L, et al. 30 Years of functionally graded materials: An overview of manufacturing methods, Applications and Future Challenges. Composites Part B: Engineering. 2020;201:108376.

[7] Mortensen A, Suresh S. Functionally graded metals and metal-ceramic composites: Part 1 Processing. International Materials Reviews. 1995;40:239-65.

[8] Yoshimi W, Hisashi S. Review Fabrication of Functionally Graded Materials under a Centrifugal Force. In: John C, editor. Nanocomposites with Unique Properties and Applications in Medicine and Industry. Rijeka: IntechOpen; 2011. p. Ch. 7.

[9] Aboudi J, Arnold SM, Pindera M-J. Response of functionally graded composites to thermal gradients. Composites Engineering. 1994;4:1-18.

[10] Shinohara Y. Chapter 11.2.4 - Functionally Graded Materials. In: Somiya S, editor. Handbook of Advanced Ceramics (Second Edition). Oxford: Academic Press; 2013. p. 1179-87.

[11] Koizumi M. FGM activities in Japan. Composites Part B: Engineering. 1997;28:1-4.

[12] Koizumi M, Niino M. Overview of FGM Research in Japan. MRS Bulletin. 1995;20:19-21.

[13] Suresh S, Mortensen A. Fundamentals of Functionally Graded Materials: Processing and Thermomechanical Behaviour of Graded Metals and Metal-ceramic Composites: IOM Communications Limited, 1998.

[14] Miyamoto Y, Kaysser WA, Rabin BH, Kawasaki A, Ford RG. Modeling and Design. In: Miyamoto Y, Kaysser WA, Rabin BH, Kawasaki A, Ford RG, editors. Functionally Graded Materials: Design, Processing and Applications. Boston, MA: Springer US; 1999. p. 63-88.

[15] Ichikawa K. Functionally Graded Materials in the 21st Century. 1st ed. New York: Springer New York, NY, 2001.

[16] Miyamoto Y, Kaysser WA, Rabin BH, Kawasaki A, Ford RG. Processing and Fabrication. In: Miyamoto Y, Kaysser WA, Rabin BH, Kawasaki A, Ford RG, editors. Functionally Graded Materials: Design, Processing and Applications. Boston, MA: Springer US; 1999. p. 161-245.

[17] Pandey PM, Rathee S, Srivastava M, Jain PK. Functionally Graded Materials (FGMs). 1st Edition ed. Boca Raton: CRC Press, 2021.

[18] Mahamood RM, Akinlabi ET. Functionally Graded Materials. 1st ed: Springer Cham, 2017.

[19] Saleh B, Jiang J, Ma A, Song D, Yang D, Xu Q. Review on the Influence of Different Reinforcements on the Microstructure and Wear Behavior of Functionally Graded Aluminum Matrix Composites by Centrifugal Casting. Metals and Materials International. 2019;26:933-60.

[20] Miao X, Sun D. Graded/Gradient Porous Biomaterials. Materials. 2010;3:26-47.

[21] Liang H, Yang Y, Xie D, Li L, Mao N, Wang C, et al. Trabecular-like Ti-6Al-4V scaffolds for orthopedic: fabrication by selective laser melting and in vitro biocompatibility. Journal of Materials Science & Technology. 2019;35:1284-97.

[22] Rabin BH, Shiota I. Functionally Gradient Materials. MRS Bulletin. 1995;20:14-8.

[23] Bever MB, Duwez PE. Gradients in composite materials. Materials Science and Engineering. 1972;10:1-8.

[24] Chan Y-S, Paulino GH, Fannjiang AC. Gradient Elasticity Theory for Mode III Fracture in Functionally Graded Materials—Part II: Crack Parallel to the Material Gradation. Journal of Applied Mechanics. 2008;75.

[25] Groves JF, Wadley HNG. Functionally graded materials synthesis via low vacuum directed vapor deposition. Composites Part B: Engineering. 1997;28:57-69.

[26] Hirai T. CVD Processing. MRS Bulletin. 1995;20:45-7.

[27] Choy KL. Chemical vapour deposition of coatings. Progress in Materials Science. 2003;48:57-170.

[28] Watanabe Y, Eryu H, Matsuura K. Evaluation of three-dimensional orientation of Al3Ti platelet in Al-based functionally graded materials fabricated by a centrifugal casting technique. Acta Materialia. 2001;49:775-83.

[29] Watanabe Y, Inaguma Y, Sato H, Miura-Fujiwara E. A Novel Fabrication Method for Functionally Graded Materials under Centrifugal Force: The Centrifugal Mixed-Powder Method. Materials2009. p. 2510-25.

[30] Haughwout LB. Centrifugal Casting Processes. In: Beadle JD, editor. Castings. London: Macmillan Education UK; 1971. p. 109-16.

[31] El-Galy IM, Saleh BI, Ahmed MH. Functionally graded materials classifications and development trends from industrial point of view. SN Applied Sciences. 2019;1:1378.

[32] Gasik M, Kawasaki A, Ueda S. Design and Powder Metallurgy Processing of Functionally Graded Materials. Materials Development and Processing - Bulk Amorphous Materials, Undercooling and Powder Metallurgy2000. p. 258-64.

[33] Kırmızı G, Arık H, Çinici H. Experimental study on mechanical and ballistic behaviours of silicon carbide reinforced functionally graded aluminum foam composites. Composites Part B: Engineering. 2019;164:345-57.

[34] Strojny-Nędza A, Pietrzak K, Węglewski W. The Influence of Al2O3 Powder Morphology on the Properties of Cu-Al2O3 Composites Designed for Functionally Graded Materials (FGM). Journal of Materials Engineering and Performance. 2016;25:3173-84.

[35] Zhu J, Lai Z, Yin Z, Jeon J, Lee S. Fabrication of ZrO2–NiCr functionally graded material by powder metallurgy. Materials Chemistry and Physics. 2001;68:130-5.

[36] Watanabe Y, Sato H, Miura-Fujiwara E. Functionally Graded Metallic Biomaterials. In: Niinomi M, Narushima T, Nakai M, editors. Advances in Metallic Biomaterials: Processing and Applications. Berlin, Heidelberg: Springer Berlin Heidelberg; 2015. p. 181-209.

[37] Loh GH, Pei E, Harrison D, Monzón MD. An overview of functionally graded additive manufacturing. Additive Manufacturing. 2018;23:34-44.

[38] Zhang C, Chen F, Huang Z, Jia M, Chen G, Ye Y, et al. Additive manufacturing of functionally graded materials: A review. Materials Science and Engineering: A. 2019;764:138209.

[39] Yap YL, Wang C, Sing SL, Dikshit V, Yeong WY, Wei J. Material jetting additive manufacturing: An experimental study using designed metrological benchmarks. Precision Engineering. 2017;50:275-85.

[40] Patricia P, Gabriel F, Olawale F, Olawale P. Laser Engineering Net Shaping Method in the Area of Development of Functionally Graded Materials (FGMs) for Aero Engine Applications - A Review. In: Mukul Chandra P, editor. Fiber Laser. Rijeka: IntechOpen; 2016. p. Ch. 17.

[41] Ngo TD, Kashani A, Imbalzano G, Nguyen KTQ, Hui D. Additive manufacturing (3D printing): A review of materials, methods, applications and challenges. Composites Part B: Engineering. 2018;143:172-96.

[42] Singh N, Singh R, Ahuja IPS. On Development of Functionally Graded Material Through Fused Deposition Modelling Assisted Investment Casting from Al2O3/SiC Reinforced Waste Low Density Polyethylene. Transactions of the Indian Institute of Metals. 2018;71:2479-85.

[43] Sireesha M, Lee J, Kranthi Kiran AS, Babu VJ, Kee BBT, Ramakrishna S. A review on additive manufacturing and its way into the oil and gas industry. RSC Advances. 2018;8:22460-8.

[44] Li W, Zhang J, Zhang X, Liou F. Effect of optimizing particle size on directed energy deposition of Functionally Graded Material with blown Pre-Mixed Multi-Powder. Manufacturing Letters. 2017;13:39-43.

[45] Stereolithography 3D Printing: From the 1980s to Now | Formlabs. https://formlabs.com/blog/history-of-stereolithography-3d-printing/. Access date: 2024/09/15/.

[46] Fused Deposition Modeling (FDM). https://www.custompartnet.com/wu/fused-deposition-modeling. Access date: 2024/09/15/.

[47] Gupta S, Chalak HD. Study on a revolutionary composite material: functionally graded material (FGM). IOP Conference Series Materials Science and Engineering. 2020;872.

[48] Sayyad AS, Ghugal YM. Modeling and analysis of functionally graded sandwich beams: a review. Mechanics of Advanced Materials and Structures. 2019;26:1776-95.

[49] Demirhan PA. Buckling Analysis of FG Timoshenko Beam Based on Physical Neutral Surface Position. Bitlis Eren Üniversitesi Fen Bilimleri Dergisi. 2024;13:633-45.

[50] Ghatage PS, Kar VR, Sudhagar PE. On the numerical modelling and analysis of multi-directional functionally graded composite structures: A review. Composite Structures. 2020;236:111837.

[51] Chi S-H, Chung Y-L. Mechanical behavior of functionally graded material plates under transverse load—Part I: Analysis. International Journal of Solids and Structures. 2006;43:3657-74.

[52] Chi S-h, Chung Y-L. Cracking in coating–substrate composites with multi-layered and FGM coatings. Engineering Fracture Mechanics. 2003;70:1227-43.

[53] Bauchau OA, Craig JI. Euler-Bernoulli beam theory. In: Bauchau OA, Craig JI, editors. Structural Analysis. Dordrecht: Springer Netherlands; 2009. p. 173-221.

[54] Öchsner A. Classical Beam Theories of Structural Mechanics. 1 ed. Switzerland: Springer Cham, 2021.
[55] Reddy JN. Theories and Analyses of Beams and Axisymmetric Circular Plates. 1st Edition ed. Boca Raton: CRC Press, 2022.
[56] Timoshenko S. History of Strength of Materials: With a Brief Account of the History of Theory of Elasticity and Theory of Structures: Dover Publications, 1983.
[57] Wang CM, Reddy JN, Lee KH. Chapter 2 - Bending of Beams. In: Wang CM, Reddy JN, Lee KH, editors. Shear Deformable Beams and Plates. Oxford: Elsevier Science Ltd; 2000. p. 11-38.
[58] Carrera E, Giunta G, Petrolo M. The Euler–Bernoulli and Timoshenko Theories. Beam Structures2011. p. 9-22.
[59] BELARBI MO. Éléments Finis pour l'Analyse des Structures Sandwichs. Biskra: Université Mohamed Khider, 2015.
[60] Hu H, Belouettar S, Potier-Ferry M, Daya EM. Review and assessment of various theories for modeling sandwich composites. Composite Structures. 2008;84:282-92.
[61] Lin X, Zhang YX, Pathak P. 2 - Finite element analysis of beams. In: Lin X, Zhang YX, Pathak P, editors. Nonlinear Finite Element Analysis of Composite and Reinforced Concrete Beams: Woodhead Publishing; 2020. p. 9-27.
[62] Rafiee M, Nitzsche F, Labrosse M. Dynamics, vibration and control of rotating composite beams and blades: A critical review. Thin-Walled Structures. 2017;119:795-819.
[63] Wang CM, Reddy JN, Lee KH. Shear Deformable Beams and Plates. In: Wang CM, Reddy JN, Lee KH, editors. Shear Deformable Beams and Plates. Oxford: Elsevier Science Ltd; 2000. p. xiii-xiv.
[64] Reddy JN. A Simple Higher-Order Theory for Laminated Composite Plates. Journal of Applied Mechanics. 1984;51:745-52.
[65] Karama M, Afaq KS, Mistou S. Mechanical behaviour of laminated composite beam by the new multi-layered laminated composite structures model with transverse shear stress continuity. International Journal of Solids and Structures. 2003;40:1525-46.
[66] Taima MS, Shehab MB, El-Sayed TA, Friswell MI. Comparative study on free vibration analysis of rotating bi-directional functionally graded beams using multiple beam theories with uncertainty considerations. Scientific Reports. 2023;13:17917.
[67] Basset AB. VI. On the extension and flexure of cylindrical and spherical thin elastic shells. Philosophical Transactions of the Royal Society of London (A). 1890;181:433-80.
[68] Hildebrand F, Reissner E, Thomas G. Notes on the foundations of the theory of small displacements of orthotropic shells. 1949.
[69] Stephen NG, Levinson M. A second order beam theory. Journal of Sound and Vibration. 1979;67:293-305.
[70] Levinson M. A new rectangular beam theory. Journal of Sound and Vibration. 1981;74:81-7.
[71] Öchsner A. Higher-Order Beam Theories. Classical Beam Theories of Structural Mechanics. Cham: Springer International Publishing; 2021. p. 105-31.
[72] SADGUI A. Modélisation du comportement des structures en Matériaux Fonctionnellement Gradués (FGM) [Doctorat]. Biskra: Université Mohamed Khider, 2022.

[73] Touratier M. An efficient standard plate theory. International Journal of Engineering Science. 1991;29:901-16.

[74] Soldatos KP. A transverse shear deformation theory for homogeneous monoclinic plates. Acta Mechanica. 1992;94:195-220.

[75] Aydogdu M. A new shear deformation theory for laminated composite plates. Composite Structures. 2009;89:94-101.

[76] Sankar BV. An elasticity solution for functionally graded beams. Composites Science and Technology. 2001;61:689-96.

[77] Huang D-j, Ding H-j, Chen W-q. Analytical solution for functionally graded anisotropic cantilever beam subjected to linearly distributed load. Applied Mathematics and Mechanics. 2007;28:855-60.

[78] Zhong Z, Yu T. Analytical solution of a cantilever functionally graded beam. Composites Science and Technology. 2007;67:481-8.

[79] Li XF. A unified approach for analyzing static and dynamic behaviors of functionally graded Timoshenko and Euler–Bernoulli beams. Journal of Sound and Vibration. 2008;318:1210-29.

[80] Benatta MA, Tounsi A, Mechab I, Bachir Bouiadjra M. Mathematical solution for bending of short hybrid composite beams with variable fibers spacing. Applied Mathematics and Computation. 2009;212:337-48.

[81] Ying J, Lü CF, Chen WQ. Two-dimensional elasticity solutions for functionally graded beams resting on elastic foundations. Composite Structures. 2008;84:209-19.

[82] Giunta G, Belouettar S, Carrera E. Analysis of FGM Beams by Means of Classical and Advanced Theories. Mechanics of Advanced Materials and Structures. 2010;17:622-35.

[83] Ma LS, Lee DW. Exact solutions for nonlinear static responses of a shear deformable FGM beam under an in-plane thermal loading. European Journal of Mechanics - A/Solids. 2012;31:13-20.

[84] Li S, Wan Z, Wang X. Homogenized and classical expressions for static bending solutions for functionally graded material Levinson beams. Applied Mathematics and Mechanics. 2015;36:895-910.

[85] Hadji L, Khelifa Z, El Abbes AB. A new higher order shear deformation model for functionally graded beams. KSCE Journal of Civil Engineering. 2016;20:1835-41.

[86] Chikh A. Analysis of static behavior of a P-FGM Beam. Journal of Materials and Engineering Structures. 2019;6:12.

[87] Apetre NA, Sankar BV, Ambur DR. Analytical Modeling of Sandwich Beams with Functionally Graded Core. Journal of Sandwich Structures & Materials. 2008;10:53-74.

[88] Venkataraman S, Sankar BV. Elasticity Solution for Stresses in a Sandwich Beam with Functionally Graded Core. AIAA Journal. 2003;41:2501-5.

[89] Zenkour AM, Allam MNM, Sobhy M. Bending analysis of FG viscoelastic sandwich beams with elastic cores resting on Pasternak's elastic foundations. Acta Mechanica. 2010;212:233-52.

[90] Fereidoon A, Andalib M, Hemmatian H. Bending Analysis of Curved Sandwich Beams with Functionally Graded Core. Mechanics of Advanced Materials and Structures. 2015;22:564-77.

[91] Kim N-I, Lee J. Exact solutions for coupled responses of thin-walled FG sandwich beams with non-symmetric cross-sections. Composites Part B: Engineering. 2017;122:121-35.

[92] Şimşek M, Al-shujairi M. Static, free and forced vibration of functionally graded (FG) sandwich beams excited by two successive moving harmonic loads. Composites Part B: Engineering. 2017;108:18-34.
[93] Kadoli R, Akhtar K, Ganesan N. Static analysis of functionally graded beams using higher order shear deformation theory. Applied Mathematical Modelling. 2008;32:2509-25.
[94] Kapuria S, Bhattacharyya M, Kumar AN. Bending and free vibration response of layered functionally graded beams: A theoretical model and its experimental validation. Composite Structures. 2008;82:390-402.
[95] Kocatürk T, Şimşek M, Akbaş ŞD. Large displacement static analysis of a cantilever Timoshenko beam composed of functionally graded material. Science and Engineering of Composite Materials. 2011;18:21-34.
[96] Mohanty SC, Dash RR, Rout T. STATIC AND DYNAMIC STABILITY ANALYSIS OF A FUNCTIONALLY GRADED TIMOSHENKO BEAM. International Journal of Structural Stability and Dynamics. 2012;12:1250025.
[97] Vo TP, Thai H-T, Nguyen T-K, Inam F. Static and vibration analysis of functionally graded beams using refined shear deformation theory. Meccanica. 2014;49:155-68.
[98] Filippi M, Carrera E, Zenkour AM. Static analyses of FGM beams by various theories and finite elements. Composites Part B: Engineering. 2015;72:1-9.
[99] Jing L-l, Ming P-j, Zhang W-p, Fu L-r, Cao Y-p. Static and free vibration analysis of functionally graded beams by combination Timoshenko theory and finite volume method. Composite Structures. 2016;138:192-213.
[100] Frikha A, Hajlaoui A, Wali M, Dammak F. A new higher order C0 mixed beam element for FGM beams analysis. Composites Part B: Engineering. 2016;106:181-9.
[101] El-Ashmawy AM, Kamel MA, Elshafei MA. Thermo-mechanical analysis of axially and transversally Function Graded Beam. Composites Part B: Engineering. 2016;102:134-49.
[102] Vo TP, Thai H-T, Nguyen T-K, Inam F, Lee J. Static behaviour of functionally graded sandwich beams using a quasi-3D theory. Composites Part B: Engineering. 2015;68:59-74.
[103] Yarasca J, Mantari JL, Arciniega RA. Hermite–Lagrangian finite element formulation to study functionally graded sandwich beams. Composite Structures. 2016;140:567-81.
[104] Karamanlı A. Bending behaviour of two directional functionally graded sandwich beams by using a quasi-3d shear deformation theory. Composite Structures. 2017;174:70-86.
[105] Kim N-I, Lee J. Flexural-torsional analysis of functionally graded sandwich I-beams considering shear effects. Composites Part B: Engineering. 2017;108:436-50.
[106] Li W, Ma H, Gao W. A higher-order shear deformable mixed beam element model for accurate analysis of functionally graded sandwich beams. Composite Structures. 2019;221:110830.
[107] Koutoati K, Mohri F, Daya EM. Finite element approach of axial bending coupling on static and vibration behaviors of functionally graded material sandwich beams. Mechanics of Advanced Materials and Structures. 2021;28:1537-53.
[108] Aydogdu M. Semi-inverse Method for Vibration and Buckling of Axially Functionally Graded Beams. Journal of Reinforced Plastics and Composites. 2008;27:683-91.

[109] Li S-R, Batra RC. Relations between buckling loads of functionally graded Timoshenko and homogeneous Euler–Bernoulli beams. Composite Structures. 2013;95:5-9.

[110] Rahimi GH, Gazor MS, Hemmatnezhad M, Toorani H. On the postbuckling and free vibrations of FG Timoshenko beams. Composite Structures. 2013;95:247-53.

[111] Nguyen T-K, Vo TP, Thai H-T. Static and free vibration of axially loaded functionally graded beams based on the first-order shear deformation theory. Composites Part B: Engineering. 2013;55:147-57.

[112] Huang Y, Zhang M, Rong H. Buckling Analysis of Axially Functionally Graded and Non-Uniform Beams Based on Timoshenko Theory. Acta Mechanica Solida Sinica. 2016;29:200-7.

[113] Trinh LC, Vo TP, Thai H-T, Nguyen T-K. An analytical method for the vibration and buckling of functionally graded beams under mechanical and thermal loads. Composites Part B: Engineering. 2016;100:152-63.

[114] Şimşek M. Buckling of Timoshenko beams composed of two-dimensional functionally graded material (2D-FGM) having different boundary conditions. Composite Structures. 2016;149:304-14.

[115] Sayyad AS, Ghugal YM. Analytical solutions for bending, buckling, and vibration analyses of exponential functionally graded higher order beams. Asian Journal of Civil Engineering. 2018;19:607-23.

[116] Kahya V, Turan M. Finite element model for vibration and buckling of functionally graded beams based on the first-order shear deformation theory. Composites Part B: Engineering. 2017;109:108-15.

[117] Farhatnia F, Sarami M. Finite element approach of bending and buckling analysis of FG beams based on refined zigzag theory. Universal Journal of Mechanical Engineering. 2019;7:147-58.

[118] Carrera E, Demirbas MD. Evaluation of bending and post-buckling behavior of thin-walled FG beams in geometrical nonlinear regime with CUF. Composite Structures. 2021;275:114408.

[119] Eslami MR, Shahsiah R, Nikbin KM. Thermal Buckling of Functionally Graded Beams. Iranian Journal of Mechanical Engineering Transactions of the ISME. 2009;10:65-81.

[120] Kiani Y, Eslami MR. Thermal buckling analysis of functionally graded material beams. International Journal of Mechanics and Materials in Design. 2010;6:229-38.

[121] Wattanasakulpong N, Gangadhara Prusty B, Kelly DW. Thermal buckling and elastic vibration of third-order shear deformable functionally graded beams. International Journal of Mechanical Sciences. 2011;53:734-43.

[122] Kiani Y, Eslami MR. Thermomechanical buckling oftemperature-dependent FGM beams. Latin American Journal of Solids and Structures. 2013;10:223-46.

[123] She G-L, Yuan F-G, Ren Y-R. Thermal buckling and post-buckling analysis of functionally graded beams based on a general higher-order shear deformation theory. Applied Mathematical Modelling. 2017;47:340-57.

[124] Alimoradzadeh M, Heidari H, Tornabene F, Dimitri R. Thermo-Mechanical Buckling and Non-Linear Free Oscillation of Functionally Graded Fiber-Reinforced Composite Laminated (FG-FRCL) Beams. Applied Sciences. 2023;13:4904.

[125] Gayen D. Thermo-elastic buckling and free vibration behavior of functionally graded beams with various materials gradation laws. International Journal on Interactive Design and Manufacturing (IJIDeM). 2024.

[126] Nguyen T-K, Truong-Phong Nguyen T, Vo TP, Thai H-T. Vibration and buckling analysis of functionally graded sandwich beams by a new higher-order shear deformation theory. Composites Part B: Engineering. 2015;76:273-85.

[127] Nguyen T-K, Vo TP, Nguyen B-D, Lee J. An analytical solution for buckling and vibration analysis of functionally graded sandwich beams using a quasi-3D shear deformation theory. Composite Structures. 2016;156:238-52.

[128] Nguyen T-K, Nguyen B-D. A new higher-order shear deformation theory for static, buckling and free vibration analysis of functionally graded sandwich beams. Journal of Sandwich Structures & Materials. 2015;17:613-31.

[129] Bennai R, Atmane HA, Tounsi A. A new higher-order shear and normal deformation theory for functionally graded sandwich beams. Steel and Composite Structures. 2015;19:521-46.

[130] Vo TP, Thai H-T, Nguyen T-K, Maheri A, Lee J. Finite element model for vibration and buckling of functionally graded sandwich beams based on a refined shear deformation theory. Engineering Structures. 2014;64:12-22.

[131] Kahya V, Turan M. Vibration and stability analysis of functionally graded sandwich beams by a multi-layer finite element. Composites Part B: Engineering. 2018;146:198-212.

[132] Fazzolari FA. Generalized exponential, polynomial and trigonometric theories for vibration and stability analysis of porous FG sandwich beams resting on elastic foundations. Composites Part B: Engineering. 2018;136:254-71.

[133] Al-shujairi M, Mollamahmutoğlu Ç. Buckling and free vibration analysis of functionally graded sandwich micro-beams resting on elastic foundation by using nonlocal strain gradient theory in conjunction with higher order shear theories under thermal effect. Composites Part B: Engineering. 2018;154:292-312.

[134] Liu Y, Su S, Huang H, Liang Y. Thermal-mechanical coupling buckling analysis of porous functionally graded sandwich beams based on physical neutral plane. Composites Part B: Engineering. 2019;168:236-42.

[135] Ellali M, Bouazza M, Amara K. Thermal buckling of a sandwich beam attached with piezoelectric layers via the shear deformation theory. Archive of Applied Mechanics. 2022;92:657-65.

[136] Aydogdu M, Taskin V. Free vibration analysis of functionally graded beams with simply supported edges. Materials & Design. 2007;28:1651-6.

[137] Sina SA, Navazi HM, Haddadpour H. An analytical method for free vibration analysis of functionally graded beams. Materials & Design. 2009;30:741-7.

[138] Chehel Amirani M, Khalili SMR, Nemati N. Free vibration analysis of sandwich beam with FG core using the element free Galerkin method. Composite Structures. 2009;90:373-9.

[139] Ait Atmane H, Tounsi A, Meftah SA, Belhadj HA. Free Vibration Behavior of Exponential Functionally Graded Beams with Varying Cross-section. Journal of Vibration and Control. 2010;17:311-8.

[140] Koochaki G. Free Vibration Analysis of Functionally Graded Beams. World Academy of Science, Engineering and Technology, International Journal of Mechanical, Aerospace, Industrial, Mechatronic and Manufacturing Engineering. 2011;5:514-7.

[141] Thai H-T, Vo TP. Bending and free vibration of functionally graded beams using various higher-order shear deformation beam theories. International Journal of Mechanical Sciences. 2012;62:57-66.

[142] Akbaş ŞD. Free vibration and bending of functionally graded beams resting on elastic foundation. Research on Engineering Structures and Materials. 2015;1:25.

[143] Hadji L, Daouadji TH, Meziane MAA, Tlidji Y, Bedia EAA. Analysis of functionally graded beam using a new first-order shear deformation theory. Structural Engineering and Mechanics. 2016;57:315-25.

[144] Wang Z-h, Wang X-h, Xu G-d, Cheng S, Zeng T. Free vibration of two-directional functionally graded beams. Composite Structures. 2016;135:191-8.

[145] Wang X, Li S. Free vibration analysis of functionally graded material beams based on Levinson beam theory. Applied Mathematics and Mechanics. 2016;37:861-78.

[146] Yildirim S. Free Vibration Analysis of Sandwich Beams with Functionally-Graded-Cores by Complementary Functions Method. AIAA Journal. 2020;58:5431-9.

[147] Doroushi A, Eslami MR, Komeili A. Vibration Analysis and Transient Response of an FGPM Beam under Thermo-Electro-Mechanical Loads using Higher-Order Shear Deformation Theory. Journal of Intelligent Material Systems and Structures. 2011;22:231-43.

[148] Alshorbagy AE, Eltaher MA, Mahmoud FF. Free vibration characteristics of a functionally graded beam by finite element method. Applied Mathematical Modelling. 2011;35:412-25.

[149] Taeprasartsit S. Nonlinear free vibration of thin functionally graded beams using the finite element method. Journal of Vibration and Control. 2015;21:29-46.

[150] Katili I, Syahril T, Katili AM. Static and free vibration analysis of FGM beam based on unified and integrated of Timoshenko's theory. Composite Structures. 2020;242:112130.

[151] Belarbi M-O, Khechai A, Houari MSA, Bessaim A, Hirane H, Garg A. Free Vibration Behavior of Sandwich FGM Beams: Parametric and Uncertainty Analysis. Journal of Vibration Engineering & Technologies. 2024.

[152] Su Z, Jin G, Wang Y, Ye X. A general Fourier formulation for vibration analysis of functionally graded sandwich beams with arbitrary boundary condition and resting on elastic foundations. Acta Mechanica. 2016;227:1493-514.

[153] Bouakkaz K, Hadji L, Zouatnia N, Adda Bedia EA. An analytical method for free vibration analysis of functionally graded sandwich beams. Wind and Structures. 2016;23:59-73.

[154] Trinh LC, Vo TP, Osofero AI, Lee J. Fundamental frequency analysis of functionally graded sandwich beams based on the state space approach. Composite Structures. 2016;156:263-75.

[155] Mashat DS, Carrera E, Zenkour AM, Al Khateeb SA, Filippi M. Free vibration of FGM layered beams by various theories and finite elements. Composites Part B: Engineering. 2014;59:269-78.

[156] Tossapanon P, Wattanasakulpong N. Stability and free vibration of functionally graded sandwich beams resting on two-parameter elastic foundation. Composite Structures. 2016;142:215-25.

[157] Bouamama M, Refassi K, Elmeiche A, Megueni A. Dynamic behavior of sandwich FGM beams. Mechanics and Mechanical Engineering. 2018;22:919-29.

[158] Akbas S. Forced vibration analysis of functionally graded sandwich deep beams. Coupled systems mechanics. 2019;8:259-71.

[159] Bhangale RK, Ganesan N. Thermoelastic buckling and vibration behavior of a functionally graded sandwich beam with constrained viscoelastic core. Journal of Sound and Vibration. 2006;295:294-316.

[160] Pradhan SC, Murmu T. Thermo-mechanical vibration of FGM sandwich beam under variable elastic foundations using differential quadrature method. Journal of Sound and Vibration. 2009;321:342-62.

[161] Rahmani M, Dehghanpour S. Temperature-Dependent Vibration of Various Types of Sandwich Beams with Porous FGM Layers. International Journal of Structural Stability and Dynamics. 2020;21:2150016.

[162] Zhang W, Wang C, Wang Y, Mao J-J, Liu Y. Nonlinear vibration responses of lattice sandwich beams with FGM facesheets based on an improved thermo-mechanical equivalent model. Structures. 2022;44:920-32.

[163] Li C, Shen H-S, Yang J. Nonlinear Vibration Behavior of FG Sandwich Beams with Auxetic Porous Copper Core in Thermal Environments. International Journal of Structural Stability and Dynamics. 2023;23:2350144.

[164] Tati A. A five unknowns high order shear deformation finite element model for functionally graded plates bending behavior analysis. Journal of the Brazilian Society of Mechanical Sciences and Engineering. 2021;43:45.

[165] Tati A. Finite element analysis of thermal and mechanical buckling behavior of functionally graded plates. Archive of Applied Mechanics. 2021;91:4571-87.

[166] Ebrahimi F, Salari E, Hosseini SAH. Thermomechanical Vibration Behavior of FG Nanobeams Subjected to Linear and Non-Linear Temperature Distributions. Journal of Thermal Stresses. 2015;38:1360-86.

[167] Sadgui A, Tati A. A novel trigonometric shear deformation theory for the buckling and free vibration analysis of functionally graded plates. Mechanics of Advanced Materials and Structures. 2022;29:6648-63.

[168] Li X-F, Wang B-L, Han J-C. A higher-order theory for static and dynamic analyses of functionally graded beams. Archive of Applied Mechanics. 2010;80:1197-212.

[169] Garg A, Chalak HD, Belarbi M-O, Chakrabarti A, Houari M-S-A. Finite Element-based Free Vibration Analysis of Power-Law, Exponential and Sigmoidal Functionally Graded Sandwich Beams. Journal of The Institution of Engineers (India): Series C. 2021;102:1167-201.

[170] Vo TP, Thai H-T, Nguyen T-K, Inam F, Lee J. A quasi-3D theory for vibration and buckling of functionally graded sandwich beams. Composite Structures. 2015;119:1-12.